Cell Reports
Methods

Article

Grabody B, an IGF1 receptor-based shuttle, mediates efficient delivery of biologics across the blood-brain barrier

Graphical abstract

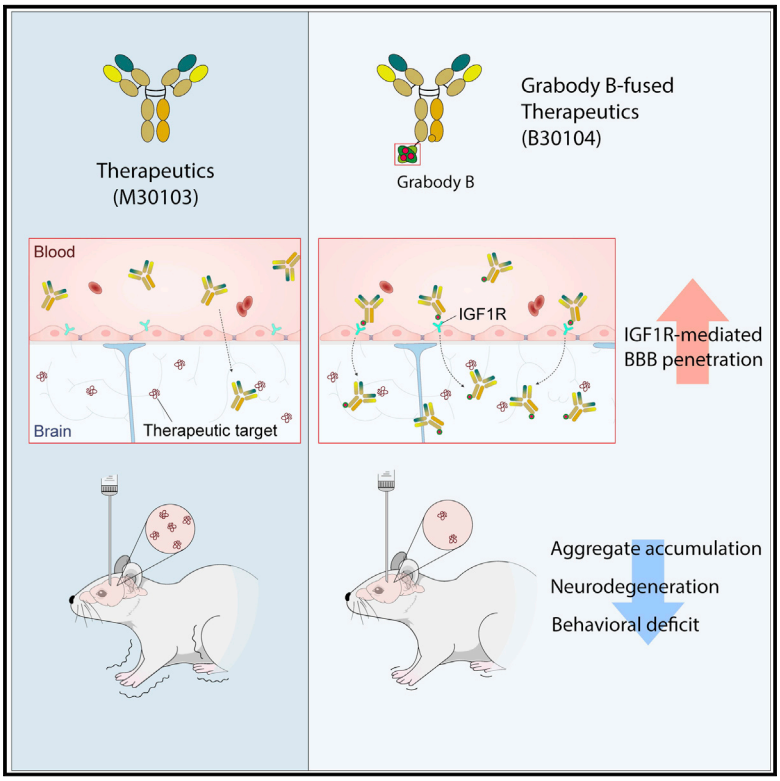

Highlights

- IGF1R is enriched higher in the CNS than in the periphery
- Grabody B, an anti-IGF1R antibody-based shuttle, does not cause safety issues in animals
- Grabody B increases the BBB penetration of antibody therapeutics
- Grabody B increases the efficacy of an anti-α-Syn antibody in a PD animal model

Authors

Jung-Won Shin, Sungwon An, Dongin Kim, ..., Sungho Maeng, Jeonghun Lee, Sang Hoon Lee

Correspondence

sungwon.an@ablbio.com (S.A.),
sang.lee@ablbio.com (S.H.L.)

In brief

Shin et al. demonstrate that Grabody B acts as a molecular shuttle to increase the BBB penetration of antibody therapeutics, which leads to increased efficacy in a disease model. Moreover, Grabody B shows improved safety in animal models.

Shin et al., 2022, Cell Reports Methods 2, 100338
November 21, 2022
https://doi.org/10.1016/j.crmeth.2022.100338

CellPress

Cell Reports Methods

CellPress
OPEN ACCESS

Article

Grabody B, an IGF1 receptor-based shuttle, mediates efficient delivery of biologics across the blood-brain barrier

Jung-Won Shin,[1,4,7] Sungwon An,[1,7,*] Dongin Kim,[1] Hyunjoo Kim,[1] Jinhyung Ahn,[1] Jaehyun Eom,[1] Weon-Kyoo You,[1] Hyesu Yun,[1] Bora Lee,[1] Byungje Sung,[1] Jinwon Jung,[1] Sehyun Kim,[1,5] Yonggyu Son,[1] Eunsil Sung,[1] Hanbyul Lee,[1] Suyeon Lee,[1] Daehae Song,[1] Youngdon Pak,[1,6] Jagdeep K. Sandhu,[2] Arsalan S. Haqqani,[2] Danica B. Stanimirovic,[2] Jiseon Yoo,[1] Donghwan Kim,[1] Sungho Maeng,[3] Jeonghun Lee,[3] and Sang Hoon Lee[1,8,*]

[1]ABL Bio, Inc., Seongnam-si, South Korea
[2]National Research Council Canada, Ottawa, ON, Canada
[3]Department of Comprehensive Health Science, Kyung Hee University, Yongin-si, South Korea
[4]Present address: 6, Central park-ro, Yeongtong-gu, Suwon-si, Gyeonggi-do, Republic of Korea
[5]Present address: Merck & Co., Inc., Kenilworth, NJ, USA
[6]Present address: IMNEWRUN Inc., Suwon-si, South Korea
[7]These authors contributed equally
[8]Lead contact
*Correspondence: sungwon.an@ablbio.com (S.A.), sang.lee@ablbio.com (S.H.L.)
https://doi.org/10.1016/j.crmeth.2022.100338

MOTIVATION To overcome the limited delivery of antibody therapeutics to the central nervous system due to the blood-brain barrier (BBB), molecular shuttles have been actively developed. The molecular shuttles were designed to bind to receptors at the surface of brain endothelial cells that are major components of the BBB. Most of the conventional molecular shuttles, however, exhibit low cross-reactivity, safety issues, or poor brain-penetrating capability. Here, we report a non-neutralizing anti-insulin-like growth factor 1 receptor (IGF1R) antibody (Grabody B) as a safe and efficient molecular shuttle that can be applicable to various therapeutic modalities for CNS-related disorders.

SUMMARY

Effective delivery of therapeutics to the brain is challenging. Molecular shuttles use receptors expressed on brain endothelial cells to deliver therapeutics. Antibodies targeting transferrin receptor (TfR) have been widely developed as molecular shuttles. However, the TfR-based approach raises concerns about safety and developmental burden. Here, we report insulin-like growth factor 1 receptor (IGF1R) as an ideal target for the molecular shuttle. We also describe Grabody B, an antibody against IGF1R, as a molecular shuttle. Grabody B has broad cross-species reactivity and does not interfere with IGF1R-mediated signaling. We demonstrate that administration of Grabody B-fused anti-alpha-synuclein (α-Syn) antibody induces better improvement in neuropathology and behavior in a Parkinson's disease animal model than the therapeutic antibody alone due to its superior serum pharmacokinetics and enhanced brain exposure. The results indicate that IGF1R is an ideal shuttle target and Grabody B is a safe and efficient molecular shuttle.

INTRODUCTION

Engineering monoclonal antibodies (mAbs) to target and neutralize neurotoxic proteinaceous species has emerged as one of the most promising strategies for treating both Alzheimer's disease (AD) (Bittar et al., 2020; Doody et al., 2014; Sevigny et al., 2016; van Dyck, 2018) and Parkinson's disease (PD) (Chatterjee and Kordower, 2019; Schwab et al., 2020; Zella et al., 2019). However, the presence of the blood-brain barrier (BBB) makes it extremely difficult to efficiently deliver therapeutic doses of large biologics, including mAbs, to the brain (Chen and Liu, 2012; Daneman and Prat, 2015; Pardridge, 2020; Stanimirovic et al., 2018).

Significant effort has been invested in developing strategies to overcome the limited delivery of biotherapeutics to the central nervous system (CNS) (Do et al., 2020; Pardridge, 2020; Yu et al., 2014). One promising approach is to take advantage of receptor-mediated transcytosis (RMT), particularly the

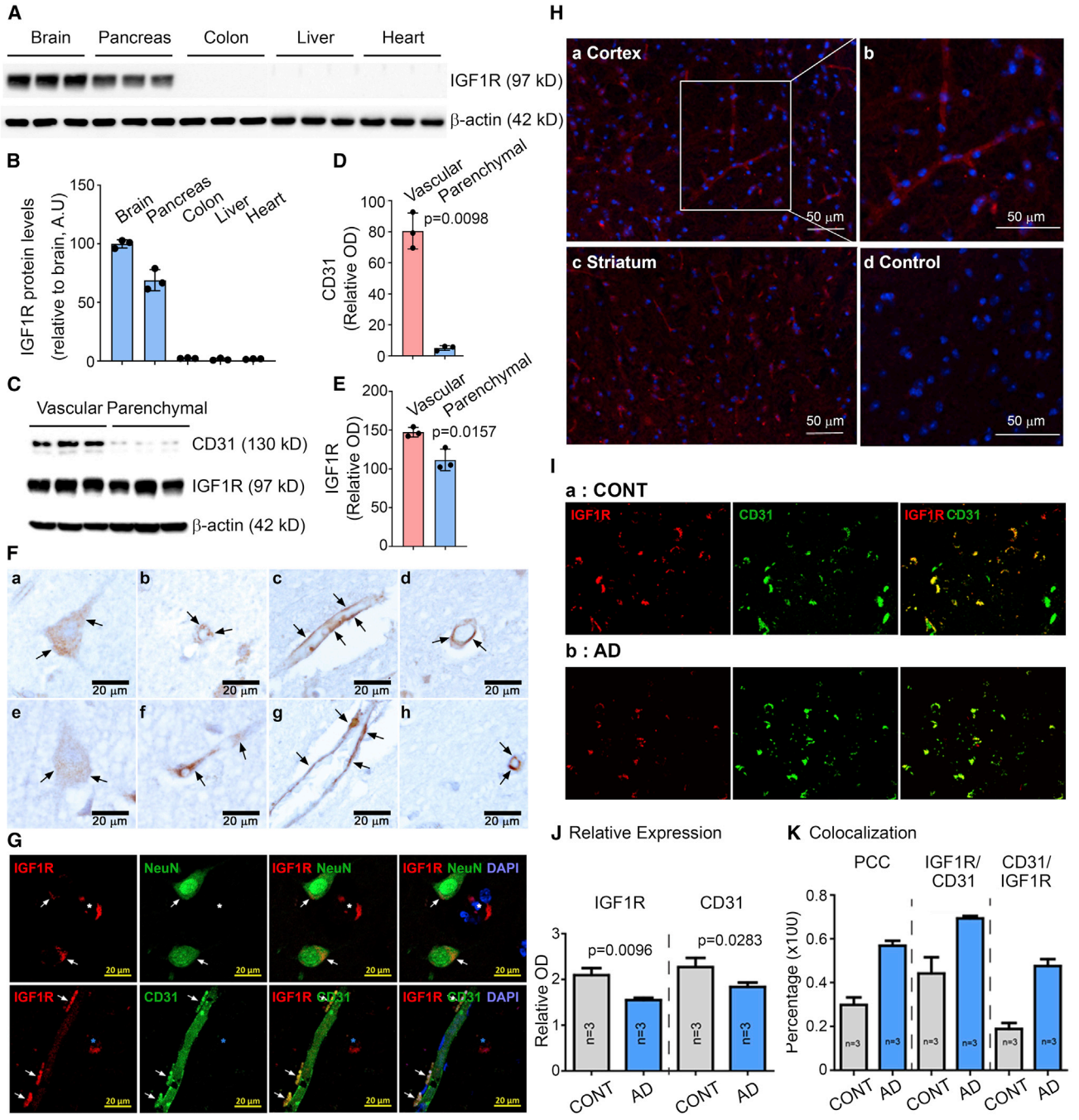

Figure 1. IGF1R is enriched in the brain and the brain vasculature

(A) Representative western blots illustrating the differences in the band intensities of IGF1R in each organ (n = 3). Note the low expression of IGF1R in the colon, liver, and heart below the detection limit. β-Actin was used as a loading control.

(B) Percentage intensity of IGF1R-immunoreactive bands normalized to the band intensity of the β-actin. n = 3 mice.

(C) IGF1R protein expression in the brain vascular or parenchymal fractions from mice. The bands are immuno-reactive to CD31, IGF1R, and β-actin in the vascular and parenchymal fractions (n = 3).

(D) Quantification of the intensity of CD31-immunoreactive bands in (C).

(E) Quantification of the intensity of IGF1R-immunoreactive bands in (C). The intensity of CD31- and IGFR-positive bands was normalized to β-actin (D and E).

(F) Representative images of human temporal lobes immuno-stained with anti-IGF1R antibody. Brain sections from three subjects showed clear expression of IGF1R in brain cells (a, e) and capillaries. BECs (b–d, f–h) are shown in brown with arrows.

(legend continued on next page)

unidirectional transcytosis pathway by which macromolecules are internalized and transported from the apical to the basolateral plasma membranes in brain endothelial cells (BECs) (Pardridge, 2020; Sehlin et al., 2020; Webster et al., 2016). As the predominant constituent of the BBB, BECs express leptin receptor (LEPR) (Golden et al., 1997), low-density lipoprotein receptor (LDLR) (Méresse et al., 1989), type 1 transferrin receptor (TfR) (Jefferies et al., 1984), and insulin receptor (IR) (Pardridge et al., 1985). Efforts have been made to utilize antibodies or peptides that bind to these various receptors as molecular shuttles for drug delivery into the brain. However, these approaches have proved to have low efficacy and often high adverse effects due to their targets' unwanted, high systemic expression outside the CNS (Couch et al., 2013; Ohshima-Hosoyama et al., 2012; Richardson and Morgan, 2004). For example, anti-TfR antibodies have been investigated as molecular shuttles, but many of these studies have shown this approach has adverse effects, ranging from anemia and lethargy to a large reduction in body temperature, in both mice (Castellanos et al., 2020; Couch et al., 2013) and non-human primates (Pardridge et al., 2018). The main cause of these effects is associated with the high expression of TfR in reticulocytes, one type of blood cell. Therefore, a receptor with expression confined more to BECs or the brain compared with the periphery may act as an ideal RMT target with a better safety profile (Stanimirovic et al., 2018; Zuchero et al., 2016).

Another drawback with current molecular shuttles is their limited cross-reactivity to either only the rodent or only the non-human primate/human brain targets, leading to increases in developmental burden (Boado et al., 2007; Castellanos et al., 2020; Paterson and Webster, 2016; Yu et al., 2014). An ideal molecular shuttle may need to be cross-reactive with various species to ensure straightforward translation of their pharmacokinetic-pharmacodynamic (PKPD) relationship across several species-derived systems (Stanimirovic et al., 2018; Webster and Stanimirovic, 2015).

Rapid clearance of the shuttle-fused therapeutic antibody poses another significant challenge of utilizing an RMT-based molecular shuttle. As a result, a shuttle-fused bispecific antibody with a shorter serum PK profile than the therapeutic antibody itself may result in only transient, not sustained, CNS exposure (Do et al., 2020; Kariolis et al., 2020; Sehlin et al., 2020; Webster et al., 2016). A shuttle-fused antibody with a prolonged serum PK profile will offer sustained antibody delivery, resulting in an overall increase in BBB penetration.

Insulin-like growth factor 1 receptor (IGF1R) is a receptor tyrosine kinase that functions in cell growth and proliferation (Ullrich et al., 1986). Its elevated expression and positive action in neoplasia are well reported in various cancers (Pollak, 2008) and have led to the development of various antibody therapeutics aimed at neutralizing the IGF1R signaling cascade (Simpson et al., 2017). In the CNS, IGF1R is known to be neuroprotective (Castilla-Cortázar et al., 2020; Gubbi et al., 2018; Selles et al., 2020). However, the IGF1R-mediated RMT mechanism has not been investigated for its utility as a shuttle to target the CNS.

Here, we report a non-neutralizing anti-IGF1R antibody, Grabody B, that has potential as a safe and efficient molecular shuttle. Unlike conventional anti-IGF1R antibodies that downregulate the IGF1R signaling axis, Grabody B does not interfere with IGF-mediated signaling and does not induce any detectable side effects. Our extensive studies have demonstrated sustained delivery of therapeutics into the brain by Grabody B, with high cross-reactivity in various species, from rodents to primates, including humans. Grabody B-fused therapeutic antibodies exhibit elevated CNS exposure compared with therapeutic antibodies alone. The Grabody B-fused anti-α-Syn antibody has an almost identical serum PK profile to therapeutic antibody alone, and achieves significantly higher therapeutic outcomes in an animal model of PD due to the elevated CNS exposure. Thus, Grabody B represents an exciting advance in the field of RMT-based therapy for neurodegenerative disorders.

RESULTS

IGF1R is enriched in the CNS and its vasculature

To compare the IGF1R expression in the brain and peripheral organs, five mouse tissues (brain, pancreas, liver, colon, and heart) were immunoblotted with a specific antibody against the 97-kDa IGF1Rβ (hereafter designated IGF1R; Figure 1A). Dense IGF1R-immunoreactive bands were observed in the brain and pancreas tissues, with little or no signal in the liver, colon, and heart. The mean ± standard error of the mean (SEM) expression relative to the brain expression normalized to β-actin (n = 3) was 1.667% ± 0.186% in the heart tissue, 2.300% ± 0.200% in the colon, 1.300% ± 0.557% in the liver, and 68.967% ± 5.189% in the pancreas (one-way ANOVA with Brown-Forsythe *post hoc*, p = 0.0006; Figures 1B, S1B, and S1C). In contrast, TfR immunoreactivity was stronger in the heart than in the brain, and TfR immunoreactivity in the liver and pancreas was comparable with the intensity in the brain (mean ± SEM [n = 3]: heart, 213.833% ± 9.967%; colon, 29.533% ± 2.784%; liver, 74.200% ± 4.460%; pancreas, 75.200% ± 8.324%; relative to brain expression; one-way ANOVA with Brown-Forsythe *post*

(G) Representative images of human temporal lobes fluorescently labeled with anti-IGF1R (red) and NeuN (green, top, a marker for mature neurons) or anti-IGF1R (red) and anti-CD31 antibodies (green, bottom). Colocalization of IGF1R and NeuN or CD31 immunoreactivity is indicated with white arrows. The blue asterisk indicates brain microvessels (top) or brain cells (bottom).
(H) Immunofluorescent detection of IGF1R in mouse brain: (a) IGF1R expression (red) in the cortex, (b) enlarged image of (a, white box) to show the presence of IGF1R in brain capillary endothelial cells, (c) IGF1R expression (red) in the striatum, (d) negative control tissue incubated with secondary antibody only. Nuclei (blue) were stained with DAPI. Scale bar, 50 μm.
(I) Representative immunofluorescent images of the human mid-frontal cortex in gray matter with AD (a) and without neurodegeneration (b) stained with anti-IGF1R and anti-CD31 antibody. n = 3 subjects per group.
(J) Quantification of the relative intensity of IGF1R (red) and CD31 (green) in control and AD brains. The relative intensity was obtained from each image and averaged together within the same group. Note that the IGF1R signal (red) highly coincides with CD31 signal (green) in AD compared with control brains (CONT).
(K) Pearson's colocalization coefficient (PCC; left bars) analysis confirmed significantly higher colocalization of CD31 and IGF1R in AD compared with CONT. Data are presented as mean ± SEM.

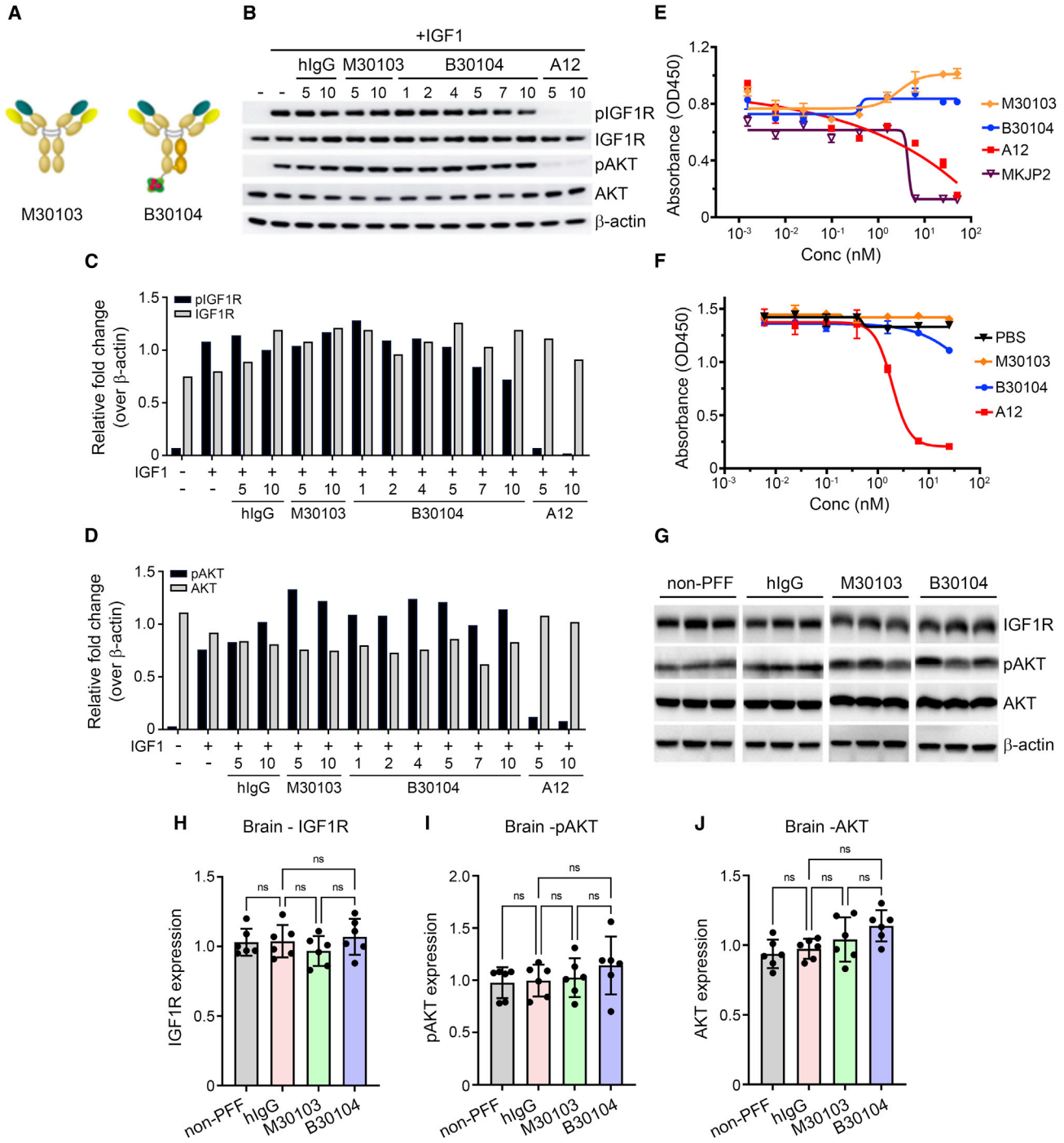

Figure 2. Grabody B does not interfere with the biological actions of IGF1R

(A) Schematic representation of M30103 and B30104. B30104 was constructed as a monovalent, bispecific antibody with an anti-α-Syn antibody (M30103) and Grabody B in an scFv format.

(B) Western blot of key IGF1R-signaling components after co-treatment of MCF7 cells with IGF1 and four different antibodies. Note the clear induction of the phosphorylation of Akt and IGF1R in the presence of IGF1 and the reduction by A12, a neutralizing anti-IGF1R antibody. In contrast, little if any alteration by M30103 or B30104 was observed.

(C and D) Relative fold intensity of pIGF1R-, IGF1R-, pAKT- and AKT-immunoreactive bands in (B). The bands were normalized to the band intensity of the β-actin. n = 3 mice.

(E) IGF1-induced MCF7 proliferation with varying concentration of four antibodies. M30103 and B30104 had a minimal effect, whereas two neutralizing anti-IGF1R antibodies (A12, red and MKJP2, magenta) inhibited cell growth. n = 3 cases. Data are presented as the mean ± SD.

(legend continued on next page)

hoc, $p < 0.0001$; Figures S1B and S1D). Using a proteomic database, we found that the brain IGF1R protein level corresponded to approximately 33% of the total IGF1R expression, in contrast to TfR, for which the brain level was 5.6% of the total expression (Figure S1A) (Wang et al., 2012). To compare the IGF1R expression level in brain vessels and parenchyma, each fraction was separated and probed with an antibody against IGF1R. Strong IGF1R immunoreactivity was observed in both fractions, but the mean ± SEM (n = 3) intensity was stronger in the vascular fraction than in the parenchyma after normalization to β-actin (147.367 ± 3.563 versus 111.600 ± 7.988; paired t test, $p = 0.0157$; Figures 1C and 1E). CD31 was highly enriched in the vascular fraction, confirming the separation of brain vessels and parenchyma (Figures 1C and 1D). These data indicate high expression of IGF1R in the brain.

We tried to visualize the IGF1R expression in murine brains by immunostaining. Mouse cortex showed strong immunoreactivity to IGF1R with clear IGF1R expression on BECs in the mouse microvasculature (Figure 1H). We further investigated the brain IGF1R expression pattern in postmortem brains, because much is unknown beyond its expression in brain cells (Moloney et al., 2010; Talbot et al., 2012). First, we identified the localization of IGF1R in human cortical sections without neurodegeneration by immuno-staining with an anti-IGF1R antibody. There was clear staining in neuronal cells (Figure 1F: a, e), which was confirmed by the colocalization of IGF1R and CD31 signals (Figure 1G). We further identified IGF1R-positive reactivity along brain microvessels, with small, globular structures decorating the vessel wall that is analogous to BECs (Figure 1F b, c, d, f, g, h, and Figure S1E). Double immunostaining of IGF1R with CD31 in the human brains further confirmed neuronal and brain microvascular expression of IGF1R (Figure 1G). This collectively suggests IGF1R expression in the brain cells and brain microvessels composed of BECs.

Next, we tried to identify the impact of aging and neurodegeneration on brain IGF1R. We measured the IGF1R protein levels by immunoblotting in postmortem human brains from subjects ranging in age from 50s to 80s. No significant differences in IGF1R levels were observed between the age groups, with the exception of a subject in the 60s with a history of diabetes (Figures S1F and S1G). We concluded that aging appears to not alter the expression of IGF1R. To examine whether IGF1R is also expressed in diseased human brain samples, we imaged medial frontal cortical sections from patients with AD and age-matched healthy controls after double immunostaining with anti-IGF1R and anti-CD31 antibodies (Figure 1I). The brain sections of both groups showed IGF1R (red) and CD31 (green) immunoreactivity, with fewer IGF1R and CD31 signals in the AD brain sections than in the control sections (unpaired t test, IGF1R, $p = 0.0096$; CD31, $p = 0.0283$; Figure 1J). Interestingly, we observed a significant increase in colocalization between IGF1R and CD31 in the AD samples. Pearson's colocalization coefficient (PCC) clearly demonstrated significantly higher co-localization of IGF1R and CD31 signals (MosaicSuite in ImageJ, AD case, $p < 0.0001$; Figure 1K). Consistent with the PCC analysis, AD brains had a higher proportion of IGF1R signal that co-localized with CD31 and CD31 signal that colocalized with IGF1R compared with control brains without neurodegeneration (unpaired t test, IGF1R/CD31, $p = 0.0014$; CD31/IGF1R, $p < 0.0001$; Figure 1K). Taken together, our results demonstrate that IGF1R is highly expressed in the brain, in both micro-blood vessels and neurons. Importantly, IGF1R expression was detected along brain microvessels in both healthy and diseased human brain samples, establishing IGF1R as an ideal candidate for an RMT shuttle.

Grabody B exhibits broad cross-species reactivity

We used surface plasmon resonance (SPR) and enzyme-linked immunosorbent assay (ELISA) to measure the binding affinity of Grabody B to the recombinant IGF1R extracellular domain (ECD) from human, monkey, rat, and mouse. Grabody B was analyzed in an scFv format fused to the C terminus of an anti-human α-Syn antibody. The sensorgrams of the SPR analysis showed a similar binding affinity of Grabody B to human and rat IGF1Rs (mean equilibrium dissociation constant [K_D] ± standard deviation [SD]: 5.435 ± 1.423 nM for human, 6.435 ± 0.180 nM for rat, 3.200 ± 0.188 nM for monkey, 0.871 ± 0.035 nM for mouse; Figure S2A). ELISA produced similar results. The half-maximal effective concentration (EC_{50}) values for Grabody B binding to the IGF1Rs from the four species were similar (0.127 nM for human, 0.289 nM for monkey, 0.397 nM for rat, 0.130 nM for mouse; Figure S2B). Therefore, Grabody B has similar binding affinities toward IGF1R from mouse, rat, monkey, and human, implying the possibility of its rapid transition from preclinical to clinical studies.

Grabody B does not alter IGF1R-mediated biology

Next, we investigated whether Grabody B binding to IGF1R interferes with IGF1-mediated signaling. We pre-treated IGF1R-expressing human breast cancer (MCF7) cells with human immunoglobulin G (hIgG), M30103 (anti-human α-Syn antibody; Figure 2A), B30104 (a monovalent bispecific antibody with M30103 and Grabody B, Figure 2A), or a neutralizing antibody against IGF1R (A12), followed by either vehicle or IGF1 treatment. The levels of IGF1R-mediated signaling pathway components (total AKT, phosphorylated Akt [pAKT (Ser473)], total IGF1R, and phosphorylated IGF1R [pIGF1R (Tyr1135/1136)]) were analyzed by western blot (Werner and LeRoith, 2014; Wrigley et al., 2017). B30104 did not affect the IGF1-induced level of pAKT or pIGF1R (Figures 2B–2D). In contrast, A12 treatment resulted in a reduction in the phosphorylation of both IGF1R and AKT. Furthermore, IGF1-induced proliferation of MCF7 cells was not affected by increasing concentrations of B30104, similar to the M30103-treated cells (Figure 2E). As expected, the two

(F) Competitive ELISA of the IGF1R-IGF1 interaction in the presence of three different antibodies or PBS control. Clear competition of A12 (red) with IGF1 was confirmed. n = 3 cases.

(G) Immunoblot of IGF1R-related signaling components from mouse brains that were chronically treated with weekly doses of hIgG or M30103 at 30 mg/kg or B30104 at 37.1 mg/kg (molar equivalent of M30103 dose) 24 times. All mice except the non-PFF control were injected with PFF.

(H–J) Quantification of the band intensity in (G). n = 6 mice. Data are presented as mean ± SD; ns, not significant.

anti-IGF1R antibodies with neutralizing activity (MKJP2 and A12) inhibited the growth of MCF7 cells in a dose-dependent manner (Figure 2E). In line with the data above, B30104 exhibited minimal if any competition with IGF1 for interaction with IGF1R, in contrast to the dose-dependent competition of A12 with IGF1 (Figure 2F). Epitope mapping of clone #1564, a parental version of Grabody B, revealed that its IGF1R binding site is distinctively separated from the IGF1 binding sites (Figures S2C and S2D). Taken together, these data indicate no interference in IGF1 binding or signaling through IGF1R by Grabody B.

To investigate whether repeated treatment with Grabody B affected the level of IGF1R *in vivo*, α-Syn pre-formed fibril (PFF)-injected mice (model details in sections "preparation of α-syn PFF and stereotaxic injection" and "Grabody B improves the efficacy of therapeutics for PD") were dosed weekly with 30 mg/kg of hIgG or M30103, or the molar equivalent of B30104 (35.1 mg/kg) for 3 months. The brain lysates were prepared and tissue collected 24 h after the last injection, followed by analysis of the total IGF1R, pAKT, and total AKT levels by western blot. The band intensity of the three signaling components did not show a significant difference between treatment groups (Figures 2G–2J). Immunoblots of the four peripheral organs (pancreas, colon, liver, and heart) from the same animals also showed overall similar band intensity for total IGF1R, pAKT, and total AKT between the treatment groups (Figures S3E–S3I). When the brain lysates were fractionated as vascular and parenchymal fractions, CD31 was highly enriched in the vascular fraction (Figures S3A and S3B), whereas IGF1R was readily detected in both fractions (mean ± SEM [n = 12 per fraction]: vascular, 144.84 ± 14.59; parenchymal, 148.62 ± 14.64; one-way ANOVA with Tukey's *post hoc*, $p > 0.05$; Figures S3A and S3C). Importantly, repeated treatment with B30104 did not result in a significant change in the vascular IGF1R level compared with the control IgG or M30103 groups (mean ± SEM [n = 3 per treatment]: IgG, 152.13 ± 3.82; M30103, 158.43 ± 7.63; B30104, 135.30 ± 8.36; one-way ANOVA with Tukey's *post hoc*, $p > 0.05$; Figure S3D). Given the presence of IGF1R expression in the pancreas and its role in glucose metabolism (Hong et al., 2017), serum glucose levels were assessed after two weekly doses of B30104 at 100 mg/kg or 200 mg/kg in rats. The serum glucose levels in the treated rats were comparable with vehicle-treated rats (mean ± SD [n = 6]: vehicle-treated males, 158.667 ± 72.666 mg/dL; 100 mg/kg B30104-treated males, 140.333 ± 39.716 mg/dL; 200 mg/kg B30104-treated males, 175.000 ± 71.014 mg/dL; vehicle-treated females, 89.667 ± 44.736 mg/dL; 100 mg/kg B30104-treated females, 146.333 ± 13.051 mg/dL; 200 mg/kg B30104-treated females, 165.333 ± 60.517 mg/dL; one-way ANOVA with Brown-Forsythe *post hoc*, $p = 0.3585$; Figure S4E). There were no B30104-induced changes in body and spleen weight (Figures S4A and S4B) or red blood cell and white blood cell counts (Figures S4C and S4D). Notably, chronic administration of B30104 with Grabody B did not induce significant weight loss, one of the common symptoms of hyperglycemia, in the PFF-injected mice compared with the hIgG- or M30103-treated groups (mean ± SEM [n = 12 per treatment], 24th week: non-PFF injected + hIgG, 42.583 ± 0.679 g; hIgG, 41.917 ± 0.580 g; M30103, 42.917 ± 1.067 g; B30104, 41.667 ± 0.501 g; ordinary one-way ANOVA, $p > 0.05$; Figure S4F).

Taken together, our results demonstrate that Grabody B does not affect the IGF1-mediated signaling pathway or its function *in vitro* or *in vivo* as demonstrated by studies on anti-IR- or anti-TfR being used as RMT shuttles (Bien-Ly et al., 2014; Couch et al., 2013; Giugliani et al., 2018).

Grabody B mediates efficient brain penetration *in vitro*

To test whether Grabody B has the ability to cross the BBB, we utilized an *in vitro* BBB model with induced BECs (iBECs) derived from amniotic fluid-derived induced pluripotent stem cells (AF-iPSCs). Using an established protocol (Ribecco-Lutkiewicz et al., 2018), human amniotic fluid cells were induced to pluripotent cells and then converted to iBECs expressing endothelial cell markers (CD31, claudin 5, and occludin; Figure S5A). M30103, M30103-1564 (clone #1564) bivalent, or B30104 was added to the iBEC monolayer in the top chamber of the transwell insert (Figure S5B). The level of each test article in the bottom chamber was quantitated by selected reaction monitoring (SRM, a method used in mass spectrometry for quantitative proteomic analysis). M30103 exhibited minimal iBEC BBB penetration, similar to the level of the negative control (A20.1). In contrast, both M30103-1564 bivalent and B30104 had significantly higher apparent permeability coefficient (Papp) values than M30103 (~4.5- and 7.3-fold, respectively; one-way ANOVA with Dunnett's T3 multiple comparison, $p < 0.0001$ in all pairs, at least three transwells per treatment; Figure S5C). B30104 had an even higher Papp value than M30103-1564 bivalent. B30104 also had higher Papp values than M30103-1564 bivalent and M30103 in a transwell assay with monolayered SV-ARBECs (immortalized rat BECs; Figure S6A) (Garberg et al., 2005).

Grabody B increases CNS exposure to therapeutic antibodies

Next, we performed intravital imaging to directly visualize Grabody B-mediated brain penetration *in vivo*. Seven-month-old mThy-1-α-syn transgenic mice overexpressing human α-Syn (Rockenstein et al., 2002) were injected with either fluorescently labeled M30103 or B30104. Alexa Fluor 555-labeled anti-CD31 antibody was co-injected to visualize brain vessels (green, Figure 3A). When the cortices were visualized immediately after injection and 6, 24, and 48 h post injection, the M30103 signals were mostly confined inside the brain vessels (top two rows, red, Figure 3A). In contrast, B30104 signals were redistributed from the vessels to the brain parenchyma starting at 24 h and persisted until 48 h (bottom two rows, red, Figure 3A). The differences between M30103 and B30104 with regard to their vascular versus parenchymal distributions were quantitated and presented in Figures 3B and 3C, respectively.

To further track the brain localization of B30104, 4-month-old female mThy-1-α-syn mice were injected intraperitoneally with 60 mg/kg of M30103 or an equal molar amount of B30104. Mice were sacrificed at 4, 24, and 72 h. Four hours post injection, a strong green signal for B30104 was seen in brain vessels compared with M30103 (arrowhead in Figure 3D, bottom panels). At 24 h, B30104 was observed throughout the sections, including the brain vessels, brain cells, and brain parenchyma, as small puncta (Figure 3D, bottom panels). At 72 h, the signal for

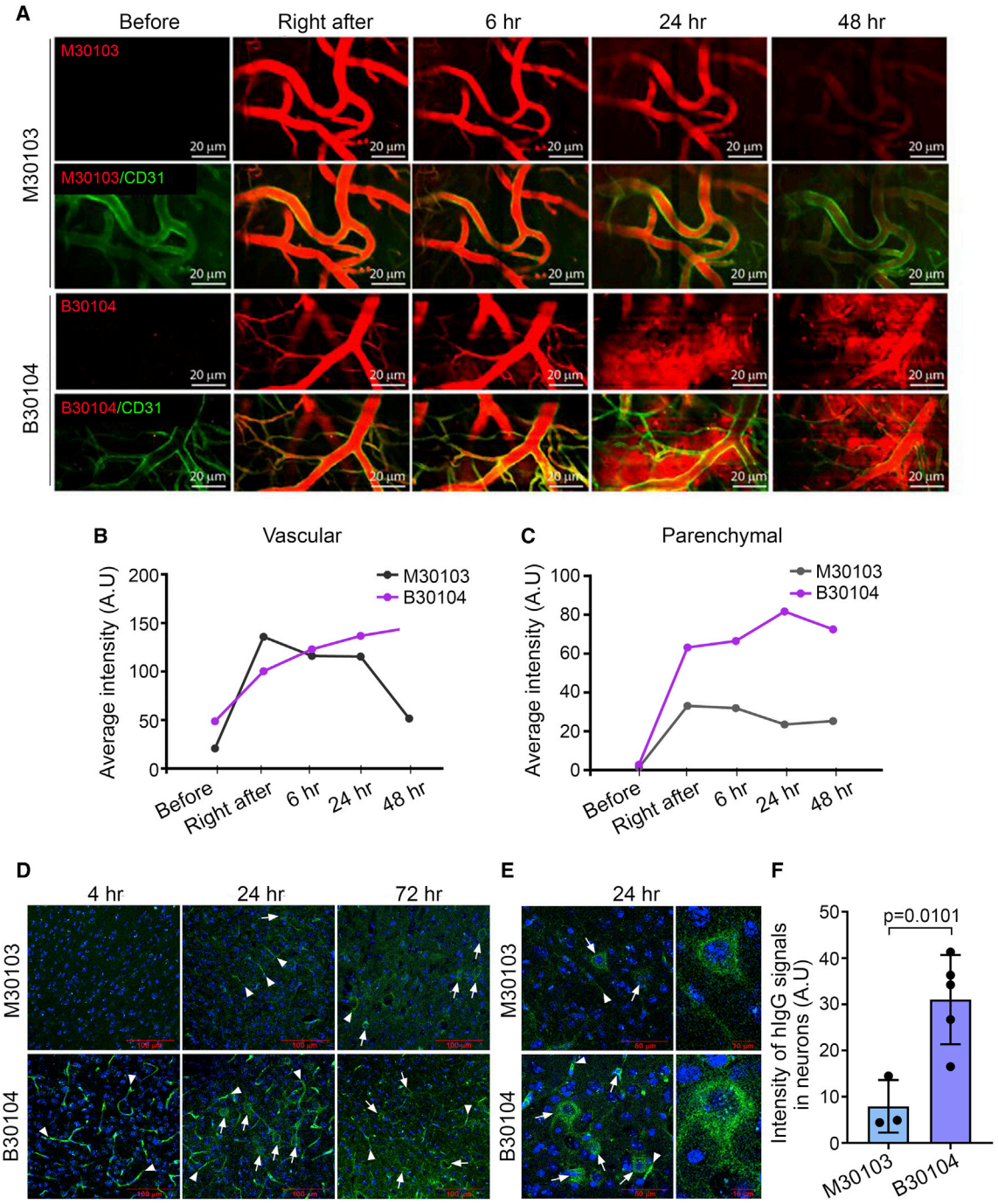

Figure 3. B30104 penetrates the brain parenchyma from brain microvessels

(A) Intravital imaging of cortical vessels after dosing male mThy-1-α-syn mice (7 months old, line 61) with fluorescently labeled M30103 or a B30104 (red) and co-injecting Alexa Fluor 555-labeled anti-CD31 antibody (green). Top, M30103; second row, merge with M30103 and anti-CD31 antibody; third row, B30104; bottom, merge with B30104 and anti-CD31 antibody. Note the sustained penetration of B30104 into the brain parenchyma from 24 h to the end of imaging (48 h), in contrast to the confinement of M30103 inside the brain microvessels during the entire imaging session. Scale bar, 20 μm.

(B and C) Quantification of the vascular and parenchymal signal intensity of M30103 or B30104.

(D) Immunostaining of brain sections from female mThy-1-α-syn mice (4 months old, line 61) after a single intraperitoneal injection of M30103 at 60 mg/kg or the same molar concentration of B30104. Note B30104's higher intensity from 4 h post injection (arrowhead, brain microvessels) to 24 and 72 h (arrowhead, brain vessels; arrows, brain cells) compared with M30103. Scale bar, 100 μm.

(E) Enlarged 24-h images of M30103- or B30104-treated brain sections (arrows, brain cells; arrowheads, brain microvessels) Scale bars, 50 or 10 μm.

(F) Quantification of the intracellular hIgG intensity in (E) with 4-fold higher hIgG intensity in the B30104 group than the M30103 group. The data are presented as mean ± SD; three cells for M30103 and five cells for B30104.

B30104 appeared to move further into the brain cells and parenchyma. In comparison, the M30103 signal was not detected at 4 h and was only weak in the vasculature and parenchyma at 24 and 72 h, respectively (Figure 3D, top panels). Although both antibodies were internalized into brain cells (Figure 3E), the intensity of the intracellular signal for B30104 was approximately 4-fold higher than the signal for M30103 (mean ± SD: M30103 [n = 3], 7.933 ± 5.692 versus B30104 [n = 5] 31.000 ± 9.659; unpaired t test, p = 0.0101; Figure 3F). Similar to the higher brain immunofluorescence (IF) signal of B30104 compared with M30103, a Grabody B-fused anti-beta-secretase 1 (BACE1) antibody exhibited an overall stronger IF signal than the anti-BACE1 antibody in multiple brain areas (Figure S7A). Collectively, we conclude that Grabody B-fused therapeutic antibodies penetrate the brain with higher efficiency than therapeutic antibodies.

Grabody B accumulates in the CNS with a significant dosing capacity

To quantify the brain penetration of and exposure to B30104, rats were intravenously injected with M30103 at a single dose of 30 mg/kg or an equal molar amount of M30103-1564 bivalent or B30104. Both the B30104 and M30103-1564 bivalent groups had significantly higher cerebrospinal fluid (CSF) and brain antibody levels than the M30103 group 24 h post injection in an LC-SRM-based analysis (one-way ANOVA with Brown-Forsythe *post hoc*; n = 3 per treatment; $p < 0.005$; Figure S6B).

Next, we measured the sustainability of B30104's CNS exposure. Rats were injected with 30 mg/kg of M30103 or an equal molar amount of B30104, and the serum, CSF, and brain levels of M30103 and B30104 up to 7 days were analyzed using LC-SRM (Figure 4A). B30104 sustainability in serum was nearly identical to that of M30103, as M30103 had a half-life of 124 h and B30104 a half-life of 119 h (Figure S6C). B30104, but not M30103, exhibited significant accumulation in both the CSF and brain (Figure 4A), with the level peaking at 24 h and then gradually declining. However, appreciable levels of B30104 were still present in both the CSF and brain 168 h following injection (mean ± SD: CSF, 2.24 ± 0.38 nM; brain, 3.69 ± 0.71 nM; Figures 4A and 4C). Importantly, when we obtained the area under the curve (AUC) of B30104 and M30103 in the CSF and brain, the AUC of B30104 was 9- to 10-fold greater than that of M30103 (Figures 4C and S6C). These data suggest that B30104 offers elevated, sustained CNS exposure up to 7 days in rodents.

The high expression of IGF1R (Figure 1) in the brain raises the possibility of antibody delivery into the brain at a significant dose by utilizing the IGF1R-based RMT. Next, we carried out a dosage study to determine the ability of B30104 to reach the CNS. Rats were intravenously injected with increasing doses of M30103 (10, 30, and 60 mg/kg or approximately 20.4, 60, 121.8 nM equivalent to 68, 200, 406 nmol/kg) or equal molar amounts of B30104 and their serum, CSF, and brain antibody levels analyzed by LC-SRM. As shown in Figure 4B, the levels of both antibodies increased similarly in a dose-dependent manner in the blood sample. However, in both the CSF and brain, a stiff linear increase was observed with increasing doses of B30104. M30103 also demonstrated a slight increase in CNS exposure. However, even at 70.2 mg/kg (same molar amount as 60 mg/kg M30103), the level of B30104 did not appear to reach saturation in either the CSF or brain (Figure 4B). At 35.1 mg/kg (same molar amount as 30 mg/kg M30103), the brain penetration of B30104 was approximately 12-fold higher than that of M30103 (Figures 4C and S6C). Taken together, these studies suggest the efficient penetration of B30104 into the brain with relatively high saturating BBB penetration mediated by Grabody B.

Grabody B improves the efficacy of therapeutics for PD

We tested whether the Grabody B-mediated RMT strategy was more efficacious than an mAb in a mouse model of PD utilizing the PFF approach (Chung et al., 2019; Rey et al., 2016; Volpicelli-Daley et al., 2011). Seven days post PFF injection, mice were treated weekly via intraperitoneal injection with 15 mg/kg of hIgG or M30103 or 17.55 mg/kg of B30104. At 180 days, the mice were assessed behaviorally and sacrificed for neuropathological analyses (Figure 5A). Mice not injected with PFF were used as a negative control.

PFF injection increased the appearance of phosphorylated α-Syn (a marker of aggregated α-Syn; p-α-Syn) (Fujiwara et al., 2002; Mao et al., 2016) in the prefrontal cortex and substantia nigra (Figure 5B). Compared with the hIgG-treated brain sections, brain sections treated with either M30103 or B30104 had a significant decrease in the number of p-α-Syn-positive cells in the prefrontal cortex (mean ± SD [n = 6 per treatment group]: hIgG, 104.300 ± 12.744 p-α-Syn-positive cells; M30103, 76.833 ± 17.025 p-α-Syn-positive cells; B30104, 42.867 ± 12.866 p-α-Syn-positive cells; Figure 5B, top row) and LB/LN-like inclusion bodies in the substantia nigra (mean ± SD [n = 6 per treatment group]: hIgG, 15.967 ± 2.921 p-α-Syn-positive cells; M30103, 11.367 ± 2.014 p-α-Syn-positive cells; B30104: 6.667 ± 3.032 p-α-Syn-positive cells; Figure 5B, bottom row). The quantitative results are shown in Figures 5C and 5D. Notably, B30104 was significantly more effective in reducing the brain p-α-Syn levels than M30103.

Next, we quantitated the number of TH-positive dopaminergic neurons in the substantia nigra pars compacta (SNpc) using an anti-tyrosine hydroxylase (TH) antibody. PFF injection appeared to significantly decrease the number of TH-positive neurons in the ipsilateral sections (Figure 6). This became evident in the ipsilateral side by comparing the high magnification images in the non-PFF group with the PFF-injected brains that received hIgG (Figures 6A–6C). Mice treated with M30103 or B30104 had more TH-positive dopaminergic neurons and denser tracts at 180 days post injection (dpi) than the hIgG control (Figure 6A). This was confirmed by quantification, which showed that B30104 treatment significantly increased the number of TH-positive neurons, whereas M30103 did not reach significance (mean ± SD [n = 6]: non-PFF 99.467% ± 11.089%; hIgG, 51.367% ± 6.315%; M30103, 61.200% ± 7.947%; B30104, 79.383% ± 5.938%; relative to TH-positive neurons in the ipsilateral SNpc; Figure 6C). Overall, PFF injection eradicated approximately 50% of the TH-positive neurons at the ipsilateral SNpc, and B30104 treatment rescued approximately 80% of the ipsilateral TH-positive neurons (mean number of TH+ neurons in SNpc ± SD [n = 6], ipsilateral versus contralateral: non-PFF, 1,248.667 ± 151.740 versus 1,237.000 ± 161.413; hIgG, 1,008.000 ± 132.558 versus 514.333 ± 67.737; M30103, 985.333 ± 156.126 versus 608.667 ± 158.187; B30104,

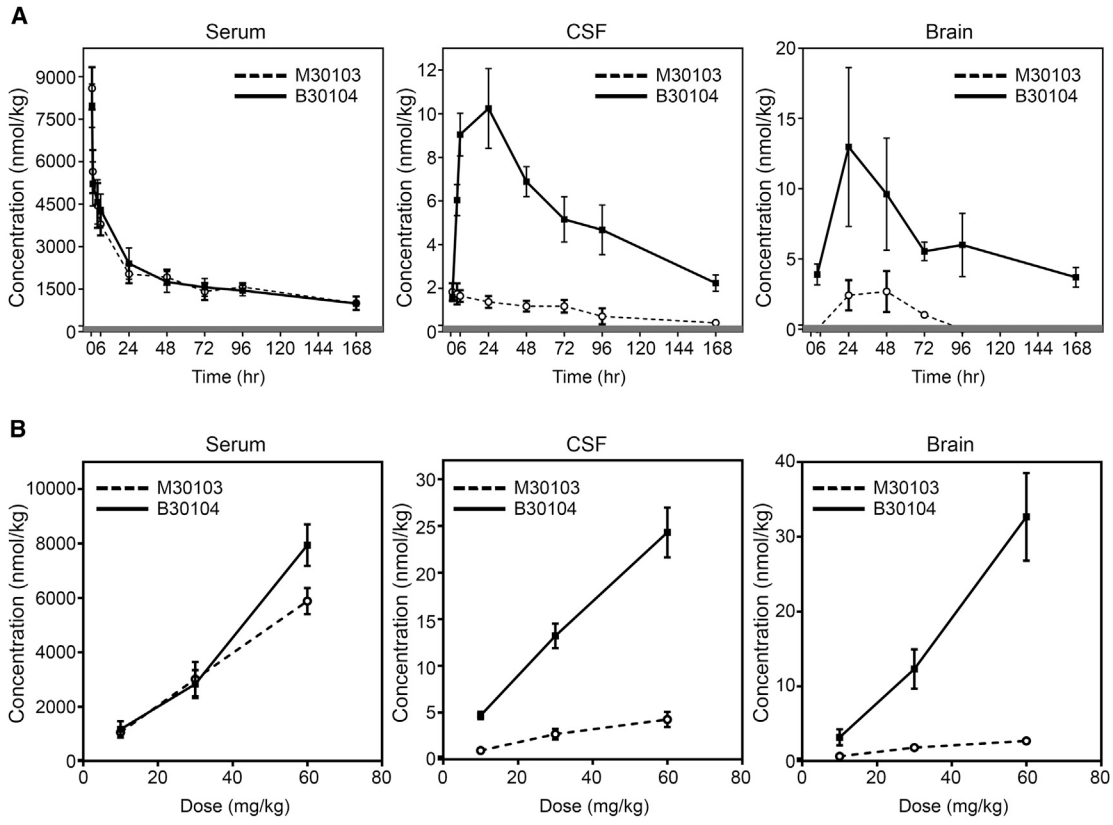

C

Ratio of B30104/M30103

mg/kg	Serum	CSF	Brain
10	1.104	4.973	4.917
30	0.940	4.894	6.864
60	1.350	5.680	12.095

Figure 4. B30104 has sustained serum and higher sustained CNS PK profiles compared with M30103 with a wide range of BBB penetration

(A) PK curves of M30103 (open circles, dashed line) and B30104 (filled squares, solid line) in serum (left), CSF (middle), and brain (right) over a 1-week period following a single 204 nmol/kg dose injected intravenously (equivalent to 30 mg/kg antibody). Data are presented as mean ± SD; six animals per time point, except three animals at 168 h.

(B) Dose-dependent curves of M30103 (open circles, dashed line) and B30104 (filled squares, solid line) in serum (left), CSF (middle), and brain (right) 24 h following a single intravenous injection of the indicated dose (10, 30, 60 mg/kg or approximately 20.4, 60, 121.8 nM antibody respectively). Note B30104's linear increase in both CSF and brain, indicative of the wide range of its CNS exposure. Data are presented as mean ± SD; three animals per dose.

(C) Fold ratio of B30104's serum, CSF, and brain levels relative to M30103 at each dose.

1001.5 ± 131.226 versus 794.833 ± 113.442; Figure 6D). These results collectively demonstrate that B30104 treatment effectively ameliorates neuropathological deficits in the PFF-injection model.

In addition, we investigated whether B30104 treatment rescues the previously reported movement-related behavioral deficits of the PFF model (Tran et al., 2014). As shown in Figures 7A and 7B, immunoblotting the insoluble fractions from the same animals for their p-α-Syn content identified three strong, dense bands larger than 15 to 20 kDa (i.e., the size of monomeric α-Syn), at roughly 50, 75, and 100 kDa, in the hIgG-treated PFF-injected group, indicating severe oligomeric p-α-Syn burden in the PFF-injected brains. Both M30103 and B30104 significantly reduced the oligomeric band intensity compared with hIgG treatment ($p < 0.001$ and $p < 0.0001$, respectively; ordinary one-way ANOVA with Tukey's multiple comparisons). The non-PFF control showed minimal band intensity (mean ± SD [n = 6 per treatment group]: hIgG, 560.48% ± 103.37%; M30103, 322.28% ± 100.48%; B30104, 232.60% ± 70.42%; relative to non-PFF). We further investigated whether B30104 administration can prevent the PFF-mediated damage to the dopaminergic system using western blot analysis to determine the levels of TH

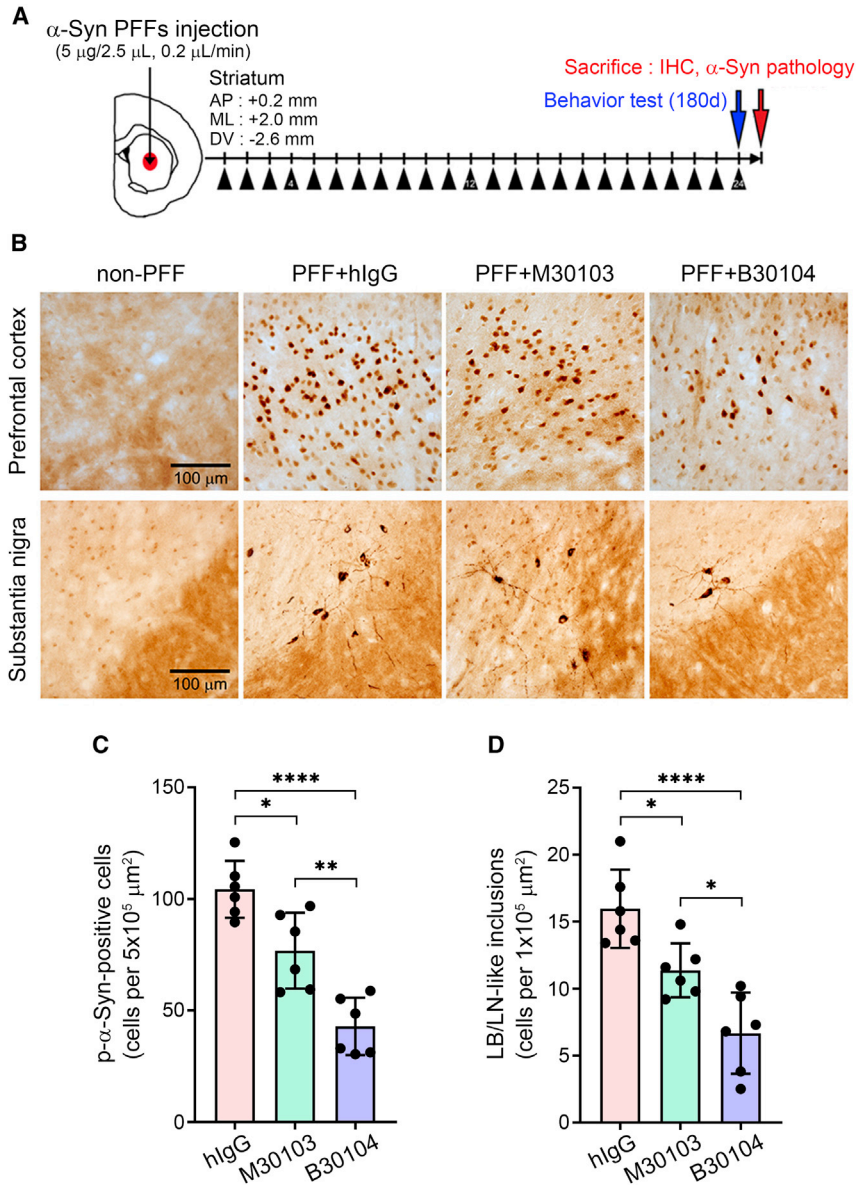

Figure 5. B30104 reduces pathological α-Syn burden more effectively than M30103

(A) Schematic of the PFF-injection efficacy test (modified from Tran et al., 2014). One week following the stereotaxic injection, the animals received 15 mg/kg of hIgG or M30103 or 17.55 mg/kg of B30104 (black triangle). The behavior of the animals was analyzed after 180 days with 24 doses and sacrificed to assess the neuropathology.

(B) Representative images of brain sections stained with anti-p-α-Syn antibody. Note the increased p-α-Syn burden 180 dpi in both the prefrontal cortex (globular or cellular type signal) and substantia nigra (cellular and fibrotic signal) of the hIgG-treated mice in contrast to the reduced p-α-Syn immunoreactivity of the M30103- or B30104-treated brains. B30104 induced further reduction of the p-α-Syn signal in both brain areas compared with M30103. Very little signal was observed in the non-PFF-injected cases. Scale bar, 100 μm.

(C and D) Quantification of the p-α-Syn-immunoreactivity in (B) as the diffused signal filling an entire cell (C, quantified as p-α-Syn-positive cells) and the number of more dense intracellular inclusions similar to Lewy bodies (LB, dense cellular inclusions filled with filamentous α-Syn aggregates found in PD brains) and Lewy neurites (LN, neurites containing filamentous similar to LB found in PD brains) (D, quantified as LB/LN-like inclusions). n = 6 mice. One-way ANOVA with Tukey's *post hoc*; *p < 0.05, **p < 0.01, ****p < 0.0001. Data are presented as mean ± SD; n = 6.

and dopamine transporter (DAT). As shown in Figures 7C–7E, striatal lysates from the PFF-injected, hIgG-treated mice had a significant reduction in the level of both TH and DAT compared with the non-PFF control striatum samples. Both M30103 and B30104 increased the density of TH- and DAT-immunoreactive bands, with a significantly greater effect of B30104 for both TH (mean ± SD [n = 6 per treatment group]: hIgG, 46.45% ± 16.99%; M30103, 57.52% ± 11.27%; B30104, 78.15% ± 22.20%; relative to non-PFF; Figures 7C and 7D) and DAT (mean ± SD [n = 6 per treatment group]: hIgG, 40.27% ± 25.71%; M30103, 44.70% ± 3.87%; B30104, 69.85% ± 3.49%; relative to non-PFF; Figures 7C and 7E). Next, we investigated whether B30104 injection also rescued behavioral deficits in the PFF mice. At both 90 and 180 dpi, mice receiving hIgG had a significant deficit in fall latency compared with the non-PFF mice in the rotarod assay. Compared with hIgG, B30104 significantly reduced the fall latency deficit at both 90 and 180 dpi, but M30103 did not (n = 12; Figure 7F). The superior efficacy of B30104 in behavioral rescue was confirmed by a wire hang test to test for grip strength, which significantly reduced the fall latency deficit at both 90 and 180 dpi (n = 12; Figure 7G). Consistent with the higher efficacy of B30104 compared with M30103, the brain's B30104 level was significantly higher than the M30103 level up to 168 h after the last dosing (mean ± SD [n = 3]: 4.873 ± 1.925 nM versus 1.027 ± 0.077 nM; two-way ANOVA; for time, p = 0.0079; between test articles, p < 0.0001; Figure S7B). Collectively, these data provide evidence of the significantly higher efficacy of B30104 in PD models than anti-α-Syn antibody due to Grabody B-mediated elevation and sustained brain penetration.

DISCUSSION

Significant effort has been invested to utilize the RMT-based mechanism to deliver therapeutic antibodies or recombinant proteins into the brain for better therapeutic efficacy. However, there are also significant concerns regarding the safety and

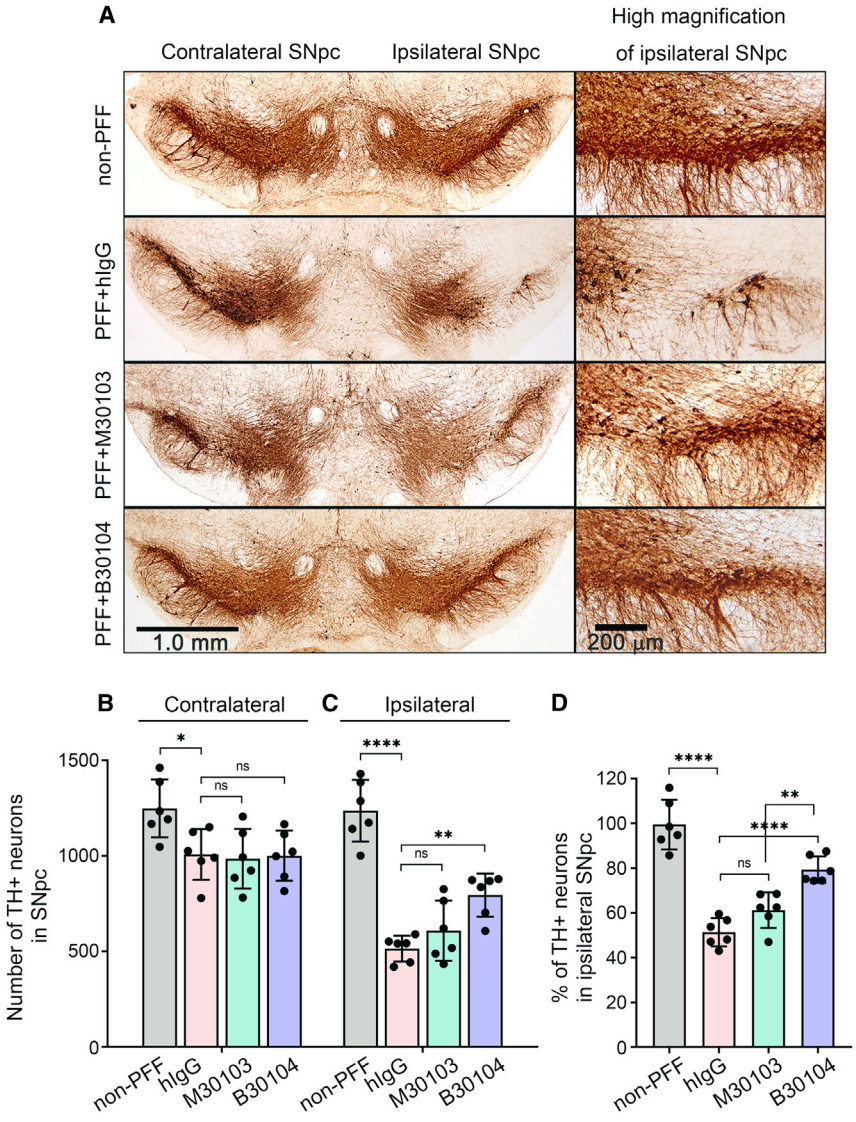

Figure 6. B30104 protects the dopaminergic system from degeneration more effectively than M30103

(A) Representative images of TH-positive dopaminergic (DA) neurons and their tracts in the ventral midbrain, including the SNpc, in PFF-injected mice at 180 dpi. High-magnification images clearly show DA neurons (round) and their tracts in the SNpc (right). PFF propagation during the 180 days induced a marked loss of DA neurons and tracts in the hIgG group's ipsilateral side. In contrast, B30104 saved the cells with tracts. Much lower efficacy of M30103 was also observed.

(B and C) Quantification of the TH-positive neurons in (A). Note the significantly higher TH-positive immunoreactivity of the B30104-treated brain than the hIgG-treated brain. M30103-treated brains had only a mild tendency for protection. No significant degeneration was observed in the contralateral side without the PFF injection and the group without PFF injection. Two-way and one-way ANOVA with Tukey's *post hoc*; $^{**}p < 0.01$, $^{****}p < 0.0001$; ns, not significant. Data are presented as mean ± SD.

(D) Relative ratio of the remaining TH-positive neurons in the SNpc. Note that ~50% of TH-positive neurons were lost by 180 dpi, and 30% of the neurons were protected by the B30104 treatment, resulting in 80% of the TH-positive neurons being present 180 dpi. Two-way and one-way ANOVA with Tukey's *post hoc*; $^{**}p < 0.01$, $^{****}p < 0.0001$; ns, not significant. Data are presented as mean ± SD; n = 6.

efficacy of current RMT technology in improving CNS exposure, as evident in early approaches using anti-TfR antibodies (Moos and Morgan, 2001; Paris-Robidas et al., 2011). Although reduced affinity or elimination of effector function can mitigate the adverse effects, reticulocyte depletion was still observed (Couch et al., 2013), possibly due to its high expression in the periphery (Figure S1) and blood (Zhang et al., 2020). Similar limitations regarding the safety or poor BBB penetration have been reported with the anti-IR antibody (Ohshima-Hosoyama et al., 2012) and an LRP-1-binding peptide (Richardson and Morgan, 2004; Zhang et al., 2020).

In this study, we demonstrated that IGF1R was predominately expressed in the brain, to a lesser extent in the pancreas, but minimally in the colon, liver, and heart. We have also shown that IGF1R is expressed in both the brain vasculature and parenchyma, in both healthy and diseased human brains, and is not affected by aging. We further showed an increase in colocalization between IGF1R and CD31 in the brain from a subject with AD. High IGF1R expression in the brain makes it possible to specifically target therapeutics to the brain with relatively high specificity. Utilizing these unique characteristics of IGF1R makes Grabody B a possibly more efficient RMT strategy than the TfR-based approach.

TfR has somewhat promiscuous expression in different tissues. According to the protein database, only 5.6% of total TfR is expressed in the human brain, whereas approximately one-third of total IGF1R is expressed in the human brain (Figure S1). We also found that TfR is highly expressed in mouse peripheral organs compared with the expression in the mouse brain. Therefore, the relative specific expression of IGF1R in the CNS was consistent with the safety profile of bispecific antibody generated with Grabody B with repeated dosing of up to 200 mg/kg in rats (Figure S4).

Currently, most TfR-based BBB shuttles, with the exception of one antibody, are not cross-reactive to both rodents and primates, including humans (Sehlin et al., 2020). Mouse and human TfR have a mere 76% similarity within coding regions (Wang et al., 2006), limiting TfR-based molecular shuttles from being tested in conventional rodent models before assessing their clinical efficacy (Sehlin et al., 2020; Stanimirovic et al., 2018). Therefore, use of knockin animals with replacement of endogenous TfR with human TfR or the use of a surrogate antibody is required

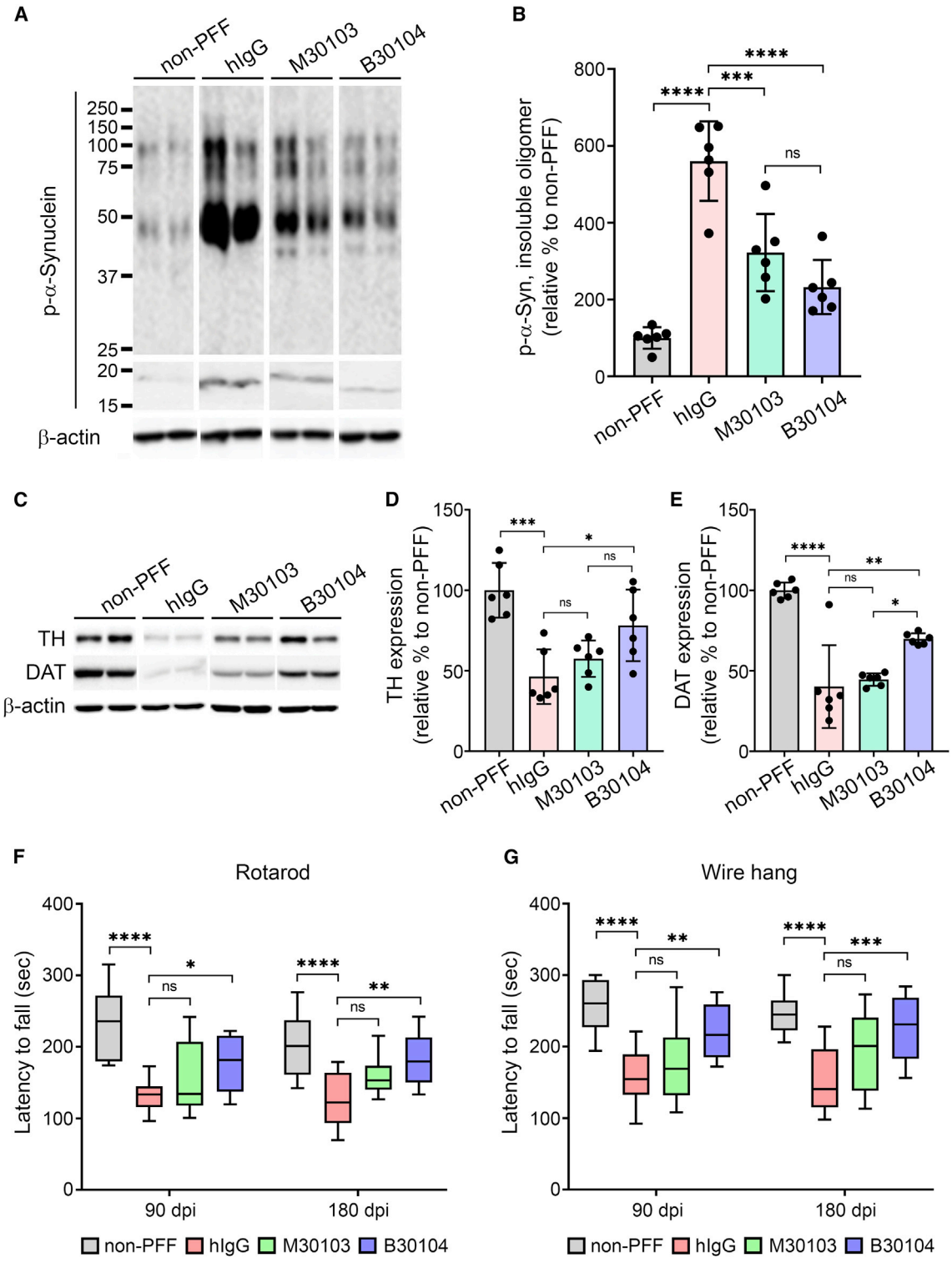

Figure 7. B30104 effectively rescues behavioral deficits by reducing pathological α-Syn and dopamine-related degeneration in the PFF-injected mouse model

(A and B) (A) P-α-Syn bands in insoluble fractions from PFF-injected mouse brains and (B) quantification of oligomeric p-α-Syn band intensity (i.e., band size larger than monomeric α-syn). Note the strong p-α-Syn oligomeric bands (three bands at approximately 100, 75, and 50 kDa) in the hIgG groups and significantly weaker immunoblot bands of the B30104-treated group. Ordinary one-way ANOVA with Tukey's multiple comparisons; ***$p < 0.001$, ****$p < 0.0001$; ns, not significant. Data are presented as mean ± SD; n = 6.

(legend continued on next page)

(Kariolis et al., 2020; Paterson and Webster, 2016; Webster and Stanimirovic, 2015; Yu et al., 2014). This will lead to additional developmental burden and difficulty translating preclinical studies in the clinic. In this regard, IGF1R has a clear benefit as a target for the transcytosis-mediated shuttle target. IGF1R has approximately 98% homology among four species: mouse, rat, monkey, and human (Gene ID: 3480). Although we could not rule out the avidity-related effect of B30104 on its binding to IGF1R, Grabody B has similar binding affinity to rodents and humans, which enables more straightforward translation of preclinical results into human brain exposure.

B30104 had a comparable serum PK profile with M30103 that contributed to sustained brain penetration and brain exposure. Interestingly, recent publications have reported the use of monovalent bispecific antibodies, although the bispecific antibodies with BBB shuttles exhibit substantially shorter serum PK profiles than mAbs (Kariolis et al., 2020). Overall, the serum PK of a bispecific antibody with a BBB shuttle appears to be dependent on the valency (Sehlin et al., 2020), the affinity of the molecular shuttle (Do et al., 2020; Thom et al., 2018; Yu et al., 2014), and the expression profile of the RMT target itself, which are known to affect the vulnerability of the antibody to systemic or intracellular degradation. In addition, when we tested the sustainability of B30104 in CNS exposure, the serum concentration of B30104 was 3,200 nM 24 h after dosing. Even 168 h after dosing, ~1,000 nM B30104 was still present in the serum with sustained brain exposure. Although we could not provide direct demonstrable ADA (anti-drug antibody, an antibody generated in the body against the infused drug that represents immunogenicity of the drug) formation in this study, our data clearly demonstrate that B30104 harboring Grabody B offers relatively high BBB penetration regardless of ADA magnitude.

BBB penetration by B30104 showed a significant dose-dependent increase from 10 to 60 mg/kg with high linearity (R^2 = 0.9952). Based on this observation, we concluded that Grabody B did not reach its saturation point at 60 mg/kg. The saturation point (more specifically, the molecular shuttle's large saturation dose) is critical in BBB penetration because the concentration of the CNS exposure limits the efficacious dose of the drug (Stocki et al., 2020; Webster et al., 2016). The M30103 levels in the CSF and brain also exhibited a minimal increase that may have originated from the limited passive flow of mAbs (Bellettato and Scarpa, 2018). Notably, the two anti-α-Syn antibodies in phase II clinical trials were dosed at ~50 mg/kg (3,500 mg, assuming an average body weight of 70 kg) (Kuchimanchi et al., 2020; Zella et al., 2019). Thus, an anti-α-Syn antibody fused with Grabody B may have improved efficacy with the same dose (i.e., 3,500 mg) in the clinic. This is further supported by our extensive demonstration of the efficacy of the molecular shuttle in a mouse PD model.

We also demonstrated the effective mobilization of Grabody B-containing bispecific antibody (B30104) into the brain parenchyma using two independent imaging technologies: intravital imaging and IF. Both analytical methods clearly showed the movement of B30104 from brain microvessels to brain parenchyma and brain cells in transgenic mice overexpressing human α-Syn. Four hours after B30104 administration, we demonstrated a strong vascular IF signal for B30104. Based on previous reports on the brain Cmax in mice at 24 h (Sehlin et al., 2020; Yu et al., 2014), the strong vascular signal of B30104 at 4 h may represent the point when B30104 is about to exit the brain vessels. This is consistent with our observation of a similar temporal profile of B30104 in the brain and CSF. Given the observation of IGF1R expression in the choroid plexus (Werner and LeRoith, 2014) and the presence of antibody in the lateral ventricle via the blood-CSF barrier as an early route to brain penetration after systemic administration (Chang et al., 2018), we speculate that the Grabody B-fused bispecific antibody could have entered both the BBB and blood-CSF barrier. Although the CSF profile of B30104 appears to be similar to its brain profile, the CSF antibody level showed relatively poor anticipation, possibly due to the higher leakiness of the choroid plexus compared with the brain (Chang et al., 2018).

Interestingly, both imaging techniques showed a sustained increase in B30104 in the parenchyma at 48 h (intravital) and 72 h (IF; Figure 3). With the evidence of enhanced brain retention of bispecific antibody harboring Grabody B that targeted BACE1 compared with its corresponding mAb (Figure S7A), we conclude that Grabody B could be applied to multiple CNS indications through multiple modalities. SRM analysis of rat brain also showed sustained brain antibody levels up to 168 h of ≥5 nM. Overall, the data indicate sustained CNS exposure by B30104 in both species, unlike bispecific antibody with a BBB shuttle with faster clearance (Sehlin et al., 2020). The sustained presence of B30104 in the brain likely contributed to the improved efficacy of the anti-α-Syn antibody in a mouse model of PD with PFF injection.

Taken together, the results suggest that IGF1R-based Grabody B represents a new RMT platform for delivering therapeutics into the brain. Our extensive studies have demonstrated that Grabody B has superior properties for crossing the BBB without adverse effects. Unlike conventional BBB shuttles, Grabody B has broad cross-reactivity with similar IGF1R binding affinity across different species. Furthermore, Grabody B-based therapy achieves significant therapeutic outcomes in an animal model of PD. These important characteristics make Grabody B an effective and versatile RMT-based platform for delivering a wide variety of therapeutics to the brain in neurodegenerative disorders.

Limitations of the study

The SRM analysis used entire brain homogenates without considering antibodies that were stuck in the vasculature, thus posing the possibility of measuring the antibody level that did

(C–E) (C) TH- and DAT-immunoreactive bands in insoluble fractions from PFF-injected mouse brains and (D and E) quantification. Ordinary one-way ANOVA with Tukey's multiple comparisons; *p < 0.05, ***p < 0.001, ****p < 0.0001; ns, not significant. Data are presented as mean ± SD; n = 6.

(F and G) Assessment of movement (balance and motor coordination) deficits measured by (F) the rotarod test and (G) wire hang test at 90 and 180 dpi. Note that only B30104 significantly improved the behavior of the animals compared with both hIgG and M30103 in both analyses. Two-way ANOVA with Bonferroni's *post hoc* test; *p < 0.05, **p < 0.01, ***p < 0.001, ****p < 0.0001; ns, not significant. Data are presented as mean ± SD; n = 12.

not yet penetrate the BBB. This may be a limitation of the current study. Nevertheless, we have ample reason to speculate that the antibody present in the brain microvessels is far less than that within the parenchyma based on our consistent observation of higher BBB penetration of B30104 and the Grabody B-fused anti-BACE1 antibody than M30103 and anti-BACE1, respectively. Future studies may need to further differentiate the BBB-penetrating antibody level between a Grabody B-fused bispecific antibody and an mAb by fractionation of vascular and parenchymal fractions (Zhang et al., 2020).

STAR★METHODS

Detailed methods are provided in the online version of this paper and include the following:

- KEY RESOURCES TABLE
- RESOURCE AVAILABILITY
  - Lead contact
  - Materials availability
  - Data and code availability
- EXPERIMENTAL MODEL AND SUBJECT DETAILS
  - Cell lines
  - Animals
  - Preparation of α-syn PFF and stereotaxic injection
  - Screening of anti-IGF1R antibodies and optimization toward Grabody B
- METHOD DETAILS
  - BBB *in vitro* transport assays using iBECs and SV-ARBECs
  - Antibody production and purification
  - Measurement of IGF1R binding affinity
  - MCF7 proliferation assay
  - IGF1-IGF1R competition assay
  - Immunofluorescent imaging of mouse brains
  - Intravital imaging
  - IGF1R epitope mapping
  - Mass spectrometry and selected reaction monitoring (SRM)
  - Immunostaining of human brains
  - Western blot
  - Treatment of PFF-injected mice
  - IHC of PFF-injected mouse brains
  - Behavioral assessments
  - Rotarod test
  - Ethical statement
- QUANTIFICATION AND STATISTICAL ANALYSIS

SUPPLEMENTAL INFORMATION

Supplemental information can be found online at https://doi.org/10.1016/j.crmeth.2022.100338.

ACKNOWLEDGMENTS

The authors thank Dr. Kyungjin Park and Juhee Kim for screening clone #1564; Dr. Chengbiao Wu, Dr. Gahee Bahn, and Dr. Hyojung Kim for manuscript review; Dr. Kijung Sung at UCSD for comments on the BBB penetration experiments; Dao Ly at NRC and Eunsin Ha for their project management; Junghyun Hong for sample purification; Seawon Ahn and Hyoju Choi for analysis of test articles; the NRC team (Eric Brunette for sample management in the SRM analysis; Christie E. Delaney for tissue homogenization and sample digestion for the SRM analysis; Claudie Charlebois for the transwell assays; Yonghong Guan for sample digestion for the SRM analysis; Alex T. Star for sample cleanup, LC-MS methods, and SRM running; Wen Ding and Xigeng Zhao for sample cleanup; Ken Chan, Sam Williamson, and Luc Tessier for MS facility maintenance for the SRM analysis; Andrew Leslie and Sue Penny for helping with data analysis regarding the BBB penetration assessment; Melissa Hewitt for technical assistance with immunofluorescent staining of mouse cortex; and Anna Jezierski for coordinating the *in vitro* BBB experiments); Dr. Doo-Jae Lee (senior research scientist) of Wide River Institute of Immunology at Seoul National University for the PFF-injected animal care; and Dr. Seung-Jae Lee for his discussion and materials for M30103 screening.

AUTHOR CONTRIBUTIONS

S.A., S.L., W.-K.Y., and H.K. conceived, designed, and planned the entire concept of the work and wrote the manuscript. J.-W.S. designed and conducted the PFF-injection model, western blot and immunohistochemistry of human brains, and immunostaining of mThy-1 brains. D.K., H.Y., Y.S., E.S., and D.K. cloned and characterized clone #1564 and its affinity variants in binding and confirmed clone #1564's and Grabody B's non-neutralizing activity. J.A., H.L., and J.E. planned and conducted an initial *in vivo* assessment of clone #1564, the rat tox study, and *in vivo* selection of 1564's affinity variants. B.L., J.J., and S.L. designed and conducted affinity maturation of the 1564 clone and its epitope mapping. B.S. corrected the amino acids of Grabody B that affect developability and conducted quality control of all materials. S.K. partially designed the study concept and wrote the manuscript. D.S., Y.P., and J.Y. designed the monovalent bispecific antibody and purified all materials. J.K.S., A.S.H., and D.B.S. immunostained IGF1R in mouse brain vessels and conducted transwell assays, the *in vivo* rat study, and the SRM analysis. S.M. and J.L. handled normal and mThy-1 α-syn mice.

DECLARATION OF INTERESTS

Authors affiliated with ABL Bio are employees with stakes in the company. The work by J.-W.S., A.S.H., and D.B.S., and the work by S.M. and J.L. described in the manuscript, was funded by ABL Bio.

Received: December 20, 2020
Revised: July 26, 2021
Accepted: October 21, 2022
Published: November 21, 2022

SUPPORTING CITATIONS

The following references appear in the supplemental information: Xu et al. (2018).

REFERENCES

Bellettato, C.M., and Scarpa, M. (2018). Possible strategies to cross the blood-brain barrier. Ital. J. Pediatr. *44*, 131.

Bien-Ly, N., Yu, Y.J., Bumbaca, D., Elstrott, J., Boswell, C.A., Zhang, Y., Luk, W., Lu, Y., Dennis, M.S., Weimer, R.M., et al. (2014). Transferrin receptor (TfR) trafficking determines brain uptake of TfR antibody affinity variants. J. Exp. Med. *211*, 233–244.

Bittar, A., Bhatt, N., and Kayed, R. (2020). Advances and considerations in AD tau-targeted immunotherapy. Neurobiol. Dis. *134*, 104707.

Boado, R.J., Zhang, Y., Zhang, Y., and Pardridge, W.M. (2007). Humanization of anti-human insulin receptor antibody for drug targeting across the human blood–brain barrier. Biotechnol. Bioeng. *96*, 381–391.

Castellanos, D.M., Sun, J., Yang, J., Ou, W., Zambon, A.C., Pardridge, W.M., and Sumbria, R.K. (2020). Acute and chronic dosing of a high-affinity

rat/mouse chimeric transferrin receptor antibody in mice. Pharmaceutics *12*, E852.

Castilla-Cortázar, I., Aguirre, G.A., Femat-Roldán, G., Martín-Estal, I., and Espinosa, L. (2020). Is insulin-like growth factor-1 involved in Parkinson's disease development? J. Transl. Med. *18*, 70.

Chang, H.Y., Morrow, K., Bonacquisti, E., Zhang, W., and Shah, D.K. (2018). Antibody pharmacokinetics in rat brain determined using microdialysis. mAbs *10*, 843–853.

Chatterjee, D., and Kordower, J.H. (2019). Immunotherapy in Parkinson's disease: current status and future directions. Neurobiol. Dis. *132*, 104587.

Chen, Y., and Liu, L. (2012). Modern methods for delivery of drugs across the blood-brain barrier. Adv. Drug Deliv. Rev. *64*, 640–665.

Chung, H.K., Ho, H.-A., Pérez-Acuña, D., and Lee, S.-J. (2019). Modeling α-synuclein propagation with preformed fibril injections. J. Mov. Disord. *12*, 139–151.

Couch, J.A., Yu, Y.J., Zhang, Y., Tarrant, J.M., Fuji, R.N., Meilandt, W.J., Solanoy, H., Tong, R.K., Hoyte, K., Luk, W., et al. (2013). Addressing safety liabilities of TfR bispecific antibodies that cross the blood-brain barrier. Sci. Transl. Med. *5*, 183ra57. 1-12-112.

Daneman, R., and Prat, A. (2015). The blood-brain barrier. Cold Spring Harbor Perspect. Biol. *7*, a020412.

Do, T.M., Capdevila, C., Pradier, L., Blanchard, V., Lopez-Grancha, M., Schussler, N., Steinmetz, A., Beninga, J., Boulay, D., Dugay, P., et al. (2020). Tetravalent bispecific tandem antibodies improve brain exposure and efficacy in an amyloid transgenic mouse model. Mol. Ther. Methods Clin. Dev. *19*, 58–77.

Doody, R.S., Thomas, R.G., Farlow, M., Iwatsubo, T., Vellas, B., Joffe, S., Kieburtz, K., Raman, R., Sun, X., Aisen, P.S., et al. (2014). Phase 3 trials of solanezumab for mild-to-moderate alzheimer's disease. N. Engl. J. Med. *370*, 311–321.

Farrington, G.K., Caram-Salas, N., Haqqani, A.S., Brunette, E., Eldredge, J., Pepinsky, B., Antognetti, G., Baumann, E., Ding, W., Garber, E., et al. (2014). A novel platform for engineering blood-brain barrier-crossing bispecific biologics. Faseb. J. *28*, 4764–4778.

Fujiwara, H., Hasegawa, M., Dohmae, N., Kawashima, A., Masliah, E., Goldberg, M.S., Shen, J., Takio, K., and Iwatsubo, T. (2002). alpha-Synuclein is phosphorylated in synucleinopathy lesions. Nat. Cell Biol. *4*, 160–164.

Garberg, P., Ball, M., Borg, N., Cecchelli, R., Fenart, L., Hurst, R.D., Lindmark, T., Mabondzo, A., Nilsson, J.E., Raub, T.J., et al. (2005). In vitro models for the blood-brain barrier. Toxicol. Vitro *19*, 299–334.

Giugliani, R., Giugliani, L., de Oliveira Poswar, F., Donis, K.C., Corte, A.D., Schmidt, M., Boado, R.J., Nestrasil, I., Nguyen, C., Chen, S., and Pardridge, W.M. (2018). Neurocognitive and somatic stabilization in pediatric patients with severe Mucopolysaccharidosis Type I after 52 weeks of intravenous brain-penetrating insulin receptor antibody-iduronidase fusion protein (valanafusp alpha): an open label phase 1-2 trial. Orphanet J. Rare Dis. *13*, 110.

Golden, P.L., Maccagnan, T.J., and Pardridge, W.M. (1997). Human blood-brain barrier leptin receptor. Binding and endocytosis in isolated human brain microvessels. J. Clin. Invest. *99*, 14–18.

Gubbi, S., Quipildor, G.F., Barzilai, N., Huffman, D.M., and Milman, S. (2018). 40 YEARS of IGF1: IGF1: the Jekyll and Hyde of the aging brain. J. Mol. Endocrinol. *61*. T171–t185.

Haqqani, A.S., Caram-Salas, N., Ding, W., Brunette, E., Delaney, C.E., Baumann, E., Boileau, E., and Stanimirovic, D. (2013). Multiplexed evaluation of serum and CSF pharmacokinetics of brain-targeting single-domain antibodies using a NanoLC-SRM-ILIS method. Mol. Pharm. *10*, 1542–1556.

Haqqani, A.S., Kelly, J.F., and Stanimirovic, D.B. (2008). Quantitative protein profiling by mass spectrometry using label-free proteomics. Methods Mol. Biol. *439*, 241–256.

Holtmaat, A., Bonhoeffer, T., Chow, D.K., Chuckowree, J., De Paola, V., Hofer, S.B., Hübener, M., Keck, T., Knott, G., Lee, W.C.A., et al. (2009). Long-term, high-resolution imaging in the mouse neocortex through a chronic cranial window. Nat. Protoc. *4*, 1128–1144.

Hong, H., Cui, Z.Z., Zhu, L., Fu, S.P., Rossi, M., Cui, Y.H., and Zhu, B.M. (2017). Central IGF1 improves glucose tolerance and insulin sensitivity in mice. Nutr. Diabetes *7*, 2.

Hubatsch, I., Ragnarsson, E.G.E., and Artursson, P. (2007). Determination of drug permeability and prediction of drug absorption in Caco-2 monolayers. Nat. Protoc. *2*, 2111–2119.

Jefferies, W.A., Brandon, M.R., Hunt, S.V., Williams, A.F., Gatter, K.C., and Mason, D.Y. (1984). Transferrin receptor on endothelium of brain capillaries. Nature *312*, 162–163.

Kariolis, M.S., Wells, R.C., Getz, J.A., Kwan, W., Mahon, C.S., Tong, R., Kim, D.J., Srivastava, A., Bedard, C., Henne, K.R., et al. (2020). Brain delivery of therapeutic proteins using an Fc fragment blood-brain barrier transport vehicle in mice and monkeys. Sci. Transl. Med. *12*, eaay1359.

Kuchimanchi, M., Monine, M., Kandadi Muralidharan, K., Woodward, C., and Penner, N. (2020). Phase II dose selection for alpha synuclein-targeting antibody cinpanemab (BIIB054) based on target protein binding levels in the brain. CPT Pharmacometrics Syst. Pharmacol. *9*, 515–522.

MacLean, B., Tomazela, D.M., Shulman, N., Chambers, M., Finney, G.L., Frewen, B., Kern, R., Tabb, D.L., Liebler, D.C., and MacCoss, M.J. (2010). Skyline: an open source document editor for creating and analyzing targeted proteomics experiments. Bioinformatics *26*, 966–968.

Mao, X., Ou, M.T., Karuppagounder, S.S., Kam, T.I., Yin, X., Xiong, Y., Ge, P., Umanah, G.E., Brahmachari, S., Shin, J.H., et al. (2016). Pathological alpha-synuclein transmission initiated by binding lymphocyte-activation gene 3. Science *353*, aah3374.

Méresse, S., Delbart, C., Fruchart, J.-C., and Cecchelli, R. (1989). Low-density lipoprotein receptor on endothelium of brain capillaries. J. Neurochem. *53*, 340–345.

Moloney, A.M., Griffin, R.J., Timmons, S., O'Connor, R., Ravid, R., and O'Neill, C. (2010). Defects in IGF-1 receptor, insulin receptor and IRS-1/2 in Alzheimer's disease indicate possible resistance to IGF-1 and insulin signalling. Neurobiol. Aging *31*, 224–243.

Moos, T., and Morgan, E.H. (2001). Restricted transport of anti-transferrin receptor antibody (OX26) through the blood–brain barrier in the rat. J. Neurochem. *79*, 119–129.

Ohshima-Hosoyama, S., Simmons, H.A., Goecks, N., Joers, V., Swanson, C.R., Bondarenko, V., Velotta, R., Brunner, K., Wood, L.D., Hruban, R.H., and Emborg, M.E. (2012). A monoclonal antibody-GDNF fusion protein is not neuroprotective and is associated with proliferative pancreatic lesions in parkinsonian monkeys. PLoS One *7*, e39036.

Pardridge, W.M. (2020). Blood-brain barrier and delivery of protein and gene therapeutics to brain. Front. Aging Neurosci. *11*, 373.

Pardridge, W.M., Boado, R.J., Patrick, D.J., Ka-Wai Hui, E., and Lu, J.Z. (2018). Blood-Brain Barrier Transport, Plasma Pharmacokinetics, and Neuropathology Following Chronic Treatment of the Rhesus Monkey with a Brain Penetrating Humanized Monoclonal Antibody Against the Human Transferrin Receptor. Mol. Pharm. *15*, 5207–5216. https://doi.org/10.1021/acs.molpharmaceut.8b00730.

Pardridge, W.M., Eisenberg, J., and Yang, J. (1985). Human blood-brain barrier insulin receptor. J. Neurochem. *44*, 1771–1778.

Paris-Robidas, S., Emond, V., Tremblay, C., Soulet, D., and Calon, F. (2011). In vivo labeling of brain capillary endothelial cells after intravenous injection of monoclonal antibodies targeting the transferrin receptor. Mol. Pharmacol. *80*, 32–39.

Paterson, J., and Webster, C.I. (2016). Exploiting transferrin receptor for delivering drugs across the blood-brain barrier. Drug Discov. Today Technol. *20*, 49–52.

Pollak, M. (2008). Insulin and insulin-like growth factor signalling in neoplasia. Nat. Rev. Cancer *8*, 915–928.

Rey, N.L., Steiner, J.A., Maroof, N., Luk, K.C., Madaj, Z., Trojanowski, J.Q., Lee, V.M.Y., and Brundin, P. (2016). Widespread transneuronal propagation of α-synucleinopathy triggered in olfactory bulb mimics prodromal Parkinson's disease. J. Exp. Med. *213*, 1759–1778.

Ribecco-Lutkiewicz, M., Sodja, C., Haukenfrers, J., Haqqani, A.S., Ly, D., Zachar, P., Baumann, E., Ball, M., Huang, J., Rukhlova, M., et al. (2018). A novel human induced pluripotent stem cell blood-brain barrier model: applicability to study antibody-triggered receptor-mediated transcytosis. Sci. Rep. *8*, 1873.

Richardson, D.R., and Morgan, E.H. (2004). The transferrin homologue, melanotransferrin (p97), is rapidly catabolized by the liver of the rat and does not effectively donate iron to the brain. Biochim. Biophys. Acta *1690*, 124–133.

Rockenstein, E., Mallory, M., Hashimoto, M., Song, D., Shults, C.W., Lang, I., and Masliah, E. (2002). Differential neuropathological alterations in transgenic mice expressing alpha-synuclein from the platelet-derived growth factor and Thy-1 promoters. J. Neurosci. Res. *68*, 568–578.

Schwab, A.D., Thurston, M.J., Machhi, J., Olson, K.E., Namminga, K.L., Gendelman, H.E., and Mosley, R.L. (2020). Immunotherapy for Parkinson's disease. Neurobiol. Dis. *137*, 104760.

Sehlin, D., Stocki, P., Gustavsson, T., Hultqvist, G., Walsh, F.S., Rutkowski, J.L., and Syvänen, S. (2020). Brain delivery of biologics using a cross-species reactive transferrin receptor 1 VNAR shuttle. Faseb. J. *34*, 13272–13283.

Selles, M.C., Fortuna, J.T.S., Zappa-Villar, M.F., de Faria, Y.P.R., Souza, A.S., Suemoto, C.K., Leite, R.E.P., Rodriguez, R.D., Grinberg, L.T., Reggiani, P.C., and Ferreira, S.T. (2020). Adenovirus-mediated transduction of insulin-like growth factor 1 protects hippocampal neurons from the toxicity of Aβ oligomers and prevents memory loss in an alzheimer mouse model. Mol. Neurobiol. *57*, 1473–1483.

Sevigny, J., Chiao, P., Bussière, T., Weinreb, P.H., Williams, L., Maier, M., Dunstan, R., Salloway, S., Chen, T., Ling, Y., et al. (2016). The antibody aducanumab reduces Aβ plaques in Alzheimer's disease. Nature *537*, 50–56.

Simpson, A., Petnga, W., Macaulay, V.M., Weyer-Czernilofsky, U., and Bogenrieder, T. (2017). Insulin-like growth factor (IGF) pathway targeting in cancer: role of the IGF Axis and opportunities for future combination studies. Targeted Oncol. *12*, 571–597.

Stanimirovic, D.B., Sandhu, J.K., and Costain, W.J. (2018). Emerging technologies for delivery of biotherapeutics and gene therapy across the blood-brain barrier. BioDrugs *32*, 547–559.

Stocki, P., Szary, J., Rasmussen, C.L.M., Demydchuk, M., Northall, L., Logan, D.B., Gauhar, A., Thei, L., Moos, T., Walsh, F.S., and Rutkowski, J.L. (2020). Blood-brain barrier transport using a high affinity, brain-selective VNAR antibody targeting transferrin receptor 1. Faseb. J. *35*, e21172.

Talbot, K., Wang, H.Y., Kazi, H., Han, L.Y., Bakshi, K.P., Stucky, A., Fuino, R.L., Kawaguchi, K.R., Samoyedny, A.J., Wilson, R.S., et al. (2012). Demonstrated brain insulin resistance in Alzheimer's disease patients is associated with IGF-1 resistance, IRS-1 dysregulation, and cognitive decline. J. Clin. Invest. *122*, 1316–1338.

Thom, G., Burrell, M., Haqqani, A.S., Yogi, A., Lessard, E., Brunette, E., Delaney, C., Baumann, E., Callaghan, D., Rodrigo, N., et al. (2018). Enhanced delivery of galanin conjugates to the brain through bioengineering of the anti-transferrin receptor antibody OX26. Mol. Pharm. *15*, 1420–1431.

Tran, H.T., Chung, C.H.Y., Iba, M., Zhang, B., Trojanowski, J.Q., Luk, K.C., and Lee, V.M.Y. (2014). Alpha-synuclein immunotherapy blocks uptake and templated propagation of misfolded alpha-synuclein and neurodegeneration. Cell Rep. *7*, 2054–2065.

Ulanet, D.B., Ludwig, D.L., Kahn, C.R., and Hanahan, D. (2010). Insulin receptor functionally enhances multistage tumor progression and conveys intrinsic resistance to IGF-1R targeted therapy. Proc. Natl. Acad. Sci. USA *107*, 10791–10798.

Ullrich, A., Gray, A., Tam, A.W., Yang-Feng, T., Tsubokawa, M., Collins, C., Henzel, W., Le Bon, T., Kathuria, S., and Chen, E. (1986). Insulin-like growth factor I receptor primary structure: comparison with insulin receptor suggests structural determinants that define functional specificity. EMBO J. *5*, 2503–2512.

van Dyck, C.H. (2018). Anti-Amyloid-β monoclonal antibodies for alzheimer's disease: pitfalls and promise. Biol. Psychiatr. *83*, 311–319.

Volpicelli-Daley, L.A., Luk, K.C., Patel, T.P., Tanik, S.A., Riddle, D.M., Stieber, A., Meaney, D.F., Trojanowski, J.Q., and Lee, V.M.Y. (2011). Exogenous α-synuclein fibrils induce Lewy body pathology leading to synaptic dysfunction and neuron death. Neuron *72*, 57–71.

Wang, E., Albritton, L., and Ross, S.R. (2006). Identification of the segments of the mouse transferrin receptor 1 required for mouse mammary tumor virus infection. J. Biol. Chem. *281*, 10243–10249.

Wang, M., Weiss, M., Simonovic, M., Haertinger, G., Schrimpf, S.P., Hengartner, M.O., and von Mering, C. (2012). PaxDb, a database of protein abundance averages across all three domains of life. Mol. Cell. Proteomics *11*, 492–500.

Webster, C.I., Caram-Salas, N., Haqqani, A.S., Thom, G., Brown, L., Rennie, K., Yogi, A., Costain, W., Brunette, E., and Stanimirovic, D.B. (2016). Brain penetration, target engagement, and disposition of the blood-brain barrier-crossing bispecific antibody antagonist of metabotropic glutamate receptor type 1. Faseb. J. *30*, 1927–1940.

Webster, C.I., and Stanimirovic, D.B. (2015). A gateway to the brain: shuttles for brain delivery of macromolecules. Ther. Deliv. *6*, 1321–1324.

Werner, H., and LeRoith, D. (2014). Insulin and insulin-like growth factor receptors in the brain: physiological and pathological aspects. Eur. Neuropsychopharmacol *24*, 1947–1953.

Wrigley, S., Arafa, D., and Tropea, D. (2017). Insulin-like growth factor 1: at the crossroads of brain development and aging. Front. Cell. Neurosci. *11*, 14.

Xu, Y., Kong, G.K.W., Menting, J.G., Margetts, M.B., Delaine, C.A., Jenkin, L.M., Kiselyov, V.V., De Meyts, P., Forbes, B.E., and Lawrence, M.C. (2018). How ligand binds to the type 1 insulin-like growth factor receptor. Nat. Commun. *9*, 821.

Yang, H.Y., Kang, K.J., Chung, J.E., and Shim, H. (2009). Construction of a large synthetic human scFv library with six diversified CDRs and high functional diversity. Mol. Cell *27*, 225–235.

Yu, Y.J., Atwal, J.K., Zhang, Y., Tong, R.K., Wildsmith, K.R., Tan, C., Bien-Ly, N., Hersom, M., Maloney, J.A., Meilandt, W.J., et al. (2014). Therapeutic bispecific antibodies cross the blood-brain barrier in nonhuman primates. Sci. Transl. Med. *6*, 261ra154.

Zella, S.M.A., Metzdorf, J., Ciftci, E., Ostendorf, F., Muhlack, S., Gold, R., and Tönges, L. (2019). Emerging immunotherapies for Parkinson disease. Neurol. Ther. *8*, 29–44.

Zhang, W., Liu, Q.Y., Haqqani, A.S., Leclerc, S., Liu, Z., Fauteux, F., Baumann, E., Delaney, C.E., Ly, D., Star, A.T., et al. (2020). Differential expression of receptors mediating receptor-mediated transcytosis (RMT) in brain microvessels, brain parenchyma and peripheral tissues of the mouse and the human. Fluids Barriers CNS *17*, 47.

Zuchero, Y.J.Y., Chen, X., Bien-Ly, N., Bumbaca, D., Tong, R.K., Gao, X., Zhang, S., Hoyte, K., Luk, W., Huntley, M.A., et al. (2016). Discovery of novel blood-brain barrier targets to enhance brain uptake of therapeutic antibodies. Neuron *89*, 70–82.

STAR★METHODS

KEY RESOURCES TABLE

REAGENT or RESOURCE	SOURCE	IDENTIFIER
Antibodies		
M30103	This paper	N/A
B30104	This paper	N/A
Anti-histidine	R&D Systems	MAB050; RRID:AB_357353
Peroxidase-conjugated anti-human IgG Fc	Pierce	N/A
Streptavidin-horse radish peroxidase	Pierce	21126
Anti-rabbit IgG Alexa Fluor 448	Thermo Scientific	A21206; RRID:AB_2535792
Anti-mouse IgG Alexa Fluor 564	Thermo Scientific	A10036; RRID:AB_2534012
AlexaFluor488 goat-anti-human secondary	Jackson	109-545-003; RRID:AB_2337831
Anti-IGF1R β	Cell Signaling	3027S; RRID:AB_2122378
Anti-IGF1Rα	Santa Cruz	sc-271606; RRID:AB_10650003
Anti-IGF1R	Santa Cruz	sc81167; RRID:AB_1124620
Anti-CD31	Abcam	28364; RRID:AB_726362
Anti-NeuN	Abcam	ab177487; RRID:AB_2532109
Phospho-AKT	Cell Signaling	9271S; RRID:AB_329825
Total AKT	Cell Signaling	9272S; RRID:AB_329827
Phospho-IGF1R	Cell Signaling	3024S; RRID:AB_331253
Total IGF1R	Cell Signaling	3018S; RRID:AB_560943
β-actin	Santa Cruz	sc-47778; RRID:AB_626632
Anti-pSer129-α-syn	Abcam	ab51253; RRID:AB_869973
Anti-tyrosine hydroxylase Ab	Pel-Freez	40101; RRID:AB_461064
Biological samples		
Human brain tissues with Alzheimer's disease	UCSD ADRC Brain Bank	X5840
Human brain tissues with Alzheimer's disease	UCSD ADRC Brain Bank	X5851
Human brain tissues with Alzheimer's disease	UCSD ADRC Brain Bank	X58733
Human brain tissues without neurodegenerative diseases	UCSD ADRC Brain Bank	X5465F
Human brain tissues without neurodegenerative diseases	UCSD ADRC Brain Bank	X5510F
Human brain tissues without neurodegenerative diseases	UCSD ADRC Brain Bank	X6870F
Human brain tissues without neurodegenerative diseases	NDRI (National Disease Research Interchange)	#2005-02407
Human brain tissues without neurodegenerative diseases	NDRI (National Disease Research Interchange)	#2005-02260
Human brain tissues without neurodegenerative diseases	NDRI (National Disease Research Interchange)	#2005-02294
Chemicals, peptides, and recombinant proteins		
Histidine-tagged human IGF1R	Sino-biological	16164-H08H
Histidine-tagged monkey IGF1R	Acro Biosystems	IGR-C5225
Histidine-tagged mouse IGF1R	R&D Systems	6630-GR-025/CF
Histidine-tagged rat IGF1R	NRC (National Research Council)	N/A
Recombinant human IGF1	R&D Systems	291-G1

(*Continued on next page*)

Continued

REAGENT or RESOURCE	SOURCE	IDENTIFIER
Human α-syn protein	rPeptide	S-1001-2
Recombinant human IGF1R extracellular domain (ECD)	R&D Systems	391-GR
TTPPVLDSDGSFFLYSK (for Fc)	NRC	N/A
ALPAPIEK (for Fc)	NRC	N/A
FNWYVDGVEVHNAK (for Fc)	NRC	N/A
GPSVFPLAPSSK (for Fab)	NRC	N/A
STSGGTAALGCLVK (for Fab)	NRC	N/A
SGTASLAISGLR (for IGF1R)	NRC	N/A
ANDYTTEYSASVK (for α-Syn)	NRC	N/A
APQVSTPTLVEAAR (for albumin)	NRC	N/A
Deposited data		
M30103	This paper	http://getentry.ddbj.nig.ac.jp/getentry/patent_aa/OF797192
B30104	This paper	http://getentry.ddbj.nig.ac.jp/getentry/patent_aa/OF797206
Experimental models: Cell lines		
OVCAR-3	ATCC®	N/A
HTB-161™	ATCC®	N/A
MCF7	ATCC®	N/A
HTB-22™	ATCC®	N/A
ExpiCHO-S™	Thermo Fisher Scientific	A29127
SV-ARBEC	Garberg et al. (2005)	N/A
Experimental models: Organism/strains		
PFF-injection mouse model	Volpicelli-Daley et al. (2011)	N/A
mThy-1-α-syn mouse	Rockenstein et al. (2002)	N/A
Mouse for PFF-injection	Japan SLC, Inc.	C57BL6/C3H, male
Rat for *in vivo* assessment of BBB penetration	Charles River Laboratories	Wistar rats, male
Other		
Phosphatase inhibitors	Roche	04693159001
Glycine-HCl	Cytiva	BR100354
1xHBS-EP	Cytiva	BR100826
Carboxyl-methyl dextran sodium salt	Sigma	86824
CCK-8 kit	Dojindo	N/A
Synthetic human scFv library (OPAL library)	Yang et al. (2009)	N/A

RESOURCE AVAILABILITY

Lead contact

Further information and requests for resources and reagents should be directed to and will be fulfilled by the lead contact, Sang Hoon Lee (sang.lee@ablbio.com).

Materials availability

- The newly generated materials in this study are mammalian and bacterial expression plasmids, monoclonal antibodies.
- The sequences of the generated materials have been deposited at DDBJ (www.ddbj.nig.ac.jp).

Data and code availability

- All original data reported in this paper are available from the lead contact upon request. The sequences of the generated materials have been deposited at DDBJ. Accession numbers are listed in the key resources table.
- This paper does not report original code.
- Any additional information required to reanalyze the data reported in this paper is available from the lead contact upon request.

EXPERIMENTAL MODEL AND SUBJECT DETAILS

Cell lines

OVCAR-3, MCF7, and ExpiCHO-S™ culture

Cells were obtained from ATCC (OVCAR-3: ATCC® HTB-161™; MCF7: ATCC® HTB-22™) or Thermo Fisher Scientific (ExpiCHO-S™ (Chinese Hamster Ovary)) and cultured following the manufacturer's standard protocols.

SV-ARBEC culture

Immortalized adult rat brain microvascular endothelial cells (SV-ARBECs) were established by SV-40 transfection of primary rat brain microvascular endothelial cells isolated from 24 to 30-day-old Sprague–Dawley rats as described previously (Garberg et al., 2005). Cells were grown in M199-based feeding media containing 0.25% peptone, 0.9% d-glucose, BME Amino Acids, BME Vitamins, and 10% FBS. Cells were routinely split 1:20 each week onto plates coated with rat-tail collagen type I (VWR, 60 μg/mL) and seeded at a density of 80,000 cells per 0.9 cm^2 of cell growth area on a 12-well Trans-well insert (1 μm pore size, BD-Falcon) coated with 60 μg/mL rat-tail collagen type I. The SV-ARBECs were cultured on the inserts for an additional 6–7 days prior to the *in vitro* transport studies.

Differentiation of human amniotic fluid-derived induced pluripotent stem cells (AF-iPSCs) into brain endothelial cells (BECs)

The human iBEC trans-well BBB model was generated as described previously (Ribecco-Lutkiewicz et al., 2018). Briefly, human iPSCs derived from human amniotic fluid cells were maintained in mTeSR1 (Stem Cell Technologies) medium until 60–70% confluence. The iPSCs were dissociated with Accutase (Stem Cell Technologies) and seeded in mTeSR1 medium at a density of 75,000 cells per well in a 6-well plate. After 2 days, the medium was changed to endothelial pre-differentiation medium (KnockOut DMEM-F12 supplemented with 20% Knockout Serum Replacement, 200 mM Glutamax, 0.1 mM NEAA, and 0.055 mM beta-mercaptoethanol; all from Life Technologies) for 6 days. The media was subsequently changed to endothelial differentiation (EM) media, which was Human Endothelial Serum-Free medium (Life Technologies) containing 1% FBS (Hyclone), 20 ng/mL bFGF (Life Technologies), and 10 μM all-*trans*-retinoic acid (Sigma Aldrich) for an additional 2 days. The iBECs were dissociated with Accutase (Stem Cell Technologies) and seeded at a density of 5×10^5 iBECs per 0.9 cm^2 of cell growth area on a 12-well trans-well insert (1 μm-pore size, BD-Falcon) coated with 80 μg/mL or 20 μg/mL collagen IV (Sigma Aldrich) in 1 mL EM medium containing 10 μM Y27362 (ROCK Inhibitor, Stem Cell Technologies). We added 2 mL of the same medium to the bottom (basal) wells of the companion plate and incubated overnight at 37°C in 5% CO_2. The following day, the EM medium in the apical compartment of the trans-well insert was replaced with EM medium without the ROCK Inhibitor and confluent monolayer formation assessed 48 h post-plating.

Animals

Male C57BL6/C3H mice (4 months old, 25–33 g) were obtained from Japan SLC, Inc. The PD transgenic mouse model that overexpresses human α-syn under the mouse Thy1 promoter (mThy-1-α-syn, Line 61) was obtained from UCSD (Rockenstein et al., 2002) under a license, bred, and maintained by Nasson Science (South Korea). Male Wistar rats aged 8–10 weeks (weight range, 230–250 g) were purchased from Charles River Laboratories International, Inc. (Wilmington, MA, USA). C57BL6/C3H mice, mThy-1-α-syn mice, and Wistar rats were used to assess *in vivo* BBB penetration. Some of the C57BL6/C3H mice received intracranial injections of pre-formed fibrils (PFFs) for the efficacy study (Figures 5, 6, and 7) and assessment of the brain, peripheral IGF1R levels (Figures 2G, S3, and S7), and *in vivo* BBB penetration following Dr. Volpicelli-Daley and her colleagues' method (see below for details). For toxicology studies, male and female Sprague-Dawley rats aged 7 weeks (weight range, 169.38–249.34 g) were purchased from Orient Bio (South Korea). Execution and ethics on animal experiment followed Nasson science's, Genia's, National Research Council Canada's, IVIM Technology's, and Kyung Hee University's Animal Care and Use Committee Approval.

Preparation of α-syn PFF and stereotaxic injection

PFF generation was performed in-house using recombinant human α-Syn protein (3 mg/mL, rPeptide, S-1001-2) according to an established method (Volpicelli-Daley et al., 2011). PFF preparations were diluted in sterile PBS and stored at −80°C. On the day of the intracranial injection, the PFFs were thawed at 37°C and triturated within a maximum of 4 h. All leftovers were discarded. Mice were initially anesthetized with ketamine hydrochloride and further maintained with 2% isoflurane in O_2-N_2O gas (Lab Animal Anesthesia System, Matrix/SurgiVet, Matrix Medical, USA). An Electronic Temperature Controller (CMA150, CMA, Sweden) was used to maintain a normal temperature range (37 ± 0.5°C). PFFs (5 μg) were injected into the striatum unilaterally (coordinates: +0.2 mm relative to Bregma, +2.0 mm from midline, +2.6 mm beneath the dura) using a 10 μL syringe (Hamilton, NV) at a rate of 0.2 μL per minute (total 2.5 μL per injection) using a micropump (Model 310, Kd Scientific, USA). Control animals received sterile PBS. The needle was maintained in place for > 5 min after completion of the PFF injection to prevent reflux, followed by its careful removal. The punctured hole in the skull was filled with bone wax and the skin sutured. The animals were monitored regularly during their recovery from surgery.

Screening of anti-IGF1R antibodies and optimization toward Grabody B

We conducted phage library screening using a synthetic human scFv library (OPAL library) against a recombinant human IGF1R extracellular domain (ECD) protein (R&D systems, 391-GR) (Yang et al., 2009). The binder clones were then screened further based on their binding to MCF7 cells that express a high level of IGF1R (Ulanet et al., 2010). Initially, clone #1564 was selected as the first

molecular shuttle based on its binding to MCF7 and *in vitro* and *in vivo* BBB penetration. We conducted affinity maturation of clone #1564 using random mutagenesis to improve its BBB penetration. One affinity variant (F06) was selected and its residues that may cause developmental burden corrected. The corrected F06 was selected as a final BBB shuttle and named Grabody B (European Patent Publication No. 3725802, International Publication No. WO2020/251316).

METHOD DETAILS

BBB *in vitro* transport assays using iBECs and SV-ARBECs

Prior to being used in the BBB permeability assays, each iBEC insert was assessed by measuring the transendothelial electrical resistance (TEER). TEER measurements were conducted on a CellZscope apparatus (Nanoanalytics) using 1-cm-diameter electrodes and standard spectrum settings: frequency 1 Hz–100 kHz, points per decade 9, and logarithmic spacing. TEER values (Ω cm^2) were calculated by subtracting TEER values for the empty inserts from the TEER values for the inserts with iBECs. The iBEC monolayers on each insert were considered intact when the TEER values were $\geq$ 300 Ω cm^2 as described previously (Ribecco-Lutkiewicz et al., 2018). The SV-ARBEC model was characterized and transport experiments performed as described previously (Garberg et al., 2005; Haqqani et al., 2013). SV-ARBEC inserts were only used in the study if sodium fluorescein permeability was $< 0.3 \times 10^{-3}$ cm/min.

The 12-well trans-well inserts (BD-Falcon) containing a confluent monolayer of iBECs or SV-ARBECs were washed three times for 5 min in wells containing 2 mL of pre-warmed HBSS to remove any residual medium. The inserts were then placed into companion plates containing 2 mL of pre-warmed transport buffer, equilibrated to 37°C in an incubator for 5–10 min, and then 500 μL of the media was carefully removed from the top (luminal) chamber of each insert and replaced with 500 μL of 2× input antibody solution. The inserts were incubated at 37°C with gentle rotation using the 311DS Labnet (Labnet International, Inc.) incubator containing an orbital shaking platform set at 20 rpm for 1 h, and 100 μL of transport buffer was collected from the bottom (abluminal) wells at 90-min intervals for the permeability analysis. Following each collection, 100 μL of pre-warmed transport buffer was added back to the bottom wells and the plates returned to the incubator.

The amount of transported antibody was assessed using sensitive SRM analysis (below) and reported as the apparent permeability coefficient (*Papp*) using the following equation:

$$Papp = \frac{dQ/dt}{Co * A}$$

Where dQ/dt is the amount of test articles in the bottom chamber, Co is initial concentration of the test articles (nmol/mL), and A is the area of the trans-well in cm^2 (Hubatsch et al., 2007).

Antibody production and purification

All antibody constructs were transiently expressed in CHO cells using the ExpiCHO™ expression system (Thermo Fisher Scientific) according to the manufacturer's protocol. The culture media was collected, centrifuged, and filtered using a 0.2-μm pore filter.

All antibody constructs were purified using the AKTA FPLC system (GE Healthcare). Briefly, harvested cell culture media was loaded onto a pre-equilibrated MabSelect SuRe column (GE Healthcare). After washing with 5 volumes of culture media (50 mM Tris-HCl, 100 mM NaCl, pH 7.2), the desired protein was eluted with 50 mM sodium citrate (pH 3.4) and immediately neutralized using 1 M Tris-base. Superdex-200 (GE Healthcare, size-exclusion chromatography) in 1× PBS (pH 7.4) was used to further improve the purity. Purified samples were dialyzed against the appropriate formulation buffer and concentrated to 5–20 mg/mL using Amicon Ultra-15 Centrifugal Filter Units 30K MWCO (EMD Millipore). The purity, host cell protein, and endotoxin content of prepared samples were routinely monitored and measured to ensure the quality of the antibodies as pre-requisite for *in vivo* analysis.

Measurement of IGF1R binding affinity

Surface plasmon resonance (SPR) measurement

SPR measurements were performed on a Biacore™ T200 instrument using CM5 (Cytiva, BR100530) immobilized with anti-histidine antibody (R&D systems, MAB050) via the amine-coupling kit (Cytiva, BR100050). Histidine-tagged IGF1R ECDs were prepared for each species (human: purchased from Sino-biological [16164-H08H]; rat: kindly provided by the National Research Council [NRC] Canada; cynomolgus monkey: purchased from Acro biosystems [IGR-C5225]; and mouse: from R&D systems [6630-GR-025/CF]). 1xHBS-EP (Cytiva, BR100826) with 20 mg/mL carboxyl-methyl dextran sodium salt (Sigma, 86824) was used as the running buffer. B30104 was serially diluted with the running buffer to a final concentration of 19.5 nM–312.5 nM. The histidine-tagged IGF1R ECDs were diluted in the running buffer and captured on the anti-histidine-coupled surface. Following the capture step, Grabody B-fused anti-α-syn antibody (B30104) was injected over the IGF1R-captured surface at a flow rate of 30 μL/min for 60 s. At the end of the sample injection, the running buffer was passed over the sensor surface for 180 s and B30104's dissociation monitored. After the dissociation, the sensor surface was regenerated with 10 mM glycine-HCl (pH 1.5; Cytiva, BR100354) at a flow rate of 30 μL/min for 30 s. Kinetic analysis was performed using the 1:1 binding model and BIAevaluation software version 01 (Cytiva). The equilibrium dissociation rate constant (K_D) was calculated from the ratio of the dissociation rate constant (Kd) divided by the association rate constant (Ka).

IGF1R binding assay

Enzyme-linked immunosorbent assays (ELISAs) were performed in 96-well Nunc-Immuno Maxi-Sorp plates (Thermo Fisher Scientific) coated with the histidine-tagged IGF1R ECDs from various species (human, mouse, and rat: same antigens as the SPR measurements; Rhesus monkey: IGF1R kindly provided by the NRC) for 16 h at 4°C. The plates were blocked with PBS containing 1% bovine serum albumin (BSA) for 2 h at 37°C. After rinsing with PBS-T (PBS containing 0.05% Tween 20) 5 times, various concentrations (400 nM–0.005 nM) of B30104 were added to each plate and then incubated for 2 h at 37°C. After washing five times with PBS-T, the bound antibodies were detected by incubation with a peroxidase-conjugated anti-human IgG Fc antibody (Pierce, 1:2000) for 1 h at 37°C. After washing with PBS-T, 100 μL of 3,3′,5,5′-tetramethylbenzidine (TMB) substrate reagent (Sigma) was added and incubated for 5 min. The reaction was stopped by adding 50 μL of 1 N sulfuric acid, and the absorbance (450–650 nm) was measured using a microplate reader (Molecular Device SpectraMax 190).

MCF7 proliferation assay

MCF7 cells were plated onto 100-mm plates and cultured in F-12/DMEM (Gibco) supplemented with 10% FBS for 24 h to reach 80% sub-confluence. An anti-α-syn Ab (M30103), B30104, or IGF1R neutralization antibodies ('A12' or 'MKJP2') were serially diluted from 25 nM to 0.006 nM in serum-free F-12/DMEM containing human IGF-1 (20 ng/well) and treated in 96-well plates (triplicate for each concentration). MCF7 cells were trypsinized and seeded onto 96-well culture plates pre-treated with each antibody (20,000 cells/well). Seventy-two hours after seeding, cell proliferation was detected by adding 10 μL of CCK-8 reagent (Dojindo), followed by incubation for 5 h at 37°C. The absorbance at 450 nm was measured using a microplate reader (Molecular Device SpectraMax 190).

IGF1-IGF1R competition assay

We coated 96-well Nunc-Immuno Maxi-Sorp plates (Thermo Scientific) with recombinant human IGF1R ECD (Sino biological, 100 ng/well) for 16 h at 4°C. The plates were then washed with PBS-T (Tween 20, 0.05%) and blocked with 1% BSA in PBS (200 μL/well) for 2 h at 37°C. Serially diluted M30103, B30104, or A12 (400 nM–0.026 nM) was added to each well (100 μL/well) and incubated for 30 min at 37°C. PBS was used as a negative control. After washing five times with PBS-T, human IGF1 that was biotinylated using the EZ-Link Sulfo-NHS-LC-Biotin kit (Thermo Fisher Scientific) was added into each well (100 ng/well) and incubated for 2 h at 37°C. The plates were further incubated with streptavidin-horseradish peroxidase (Pierce, Cat: #21126, 1:5,000 from 1 mg/mL stock, 20 ng/well) for 1 h at 37°C. After washing with PBS-T, the plates were incubated with 100 μL of TMB substrate reagent (Sigma) for 5 min. The calorimetric reaction was measured using a microplate reader (Molecular Device SpectraMax 190) at 450–650 nm after the addition of 50 μL of 1 N sulfuric acid.

Immunofluorescent imaging of mouse brains

Detection of IGF1R in mouse brain

Mice were anesthetized by isoflurane inhalation and transcardially perfused with 0.9% saline. Their brains were removed and cut along the coronal plane. Each quarter of the brain was embedded in Optimal Cutting Temperature (OCT) compound, frozen over isopentane/dry ice, and stored at −80°C until sectioning. Coronal cryostat sections (12 μm) were collected on Superfrost Plus glass slides, followed by fixation in formalin-free 1× zinc fixative prepared from a 10× stock (Becton, Dickinson and Company, Franklin Lakes, NJ, USA). Sections were washed with PBS (Wisent Inc) containing 0.05% Tween-20, followed by permeabilization with 0.3% Triton X-100 for 15 min at room temperature (RT). Non-specific immunoglobulins were blocked with Dako serum-free protein block (Dako) for 1 h at RT. Excess protein block was removed and sections incubated overnight on a shaker at 4°C with rabbit polyclonal antibody to IGF1R β (1:100 dilution in Dako antibody diluent; #3027S, Cell Signaling Technology). Sections were washed three times (2 min each) with Tris-buffered saline (TBS, Dako), and then incubated with biotinylated goat anti-rabbit IgG (1:150 dilution in Dako antibody diluent; Vector Laboratories) for 45 min at RT. Sections were washed three times (2 min each) and the biotinylated conjugates detected by incubation with 1:400 streptavidin conjugated to Cy3 (SA-Cy3, Jackson Immunoresearch) for 30 min at RT. Sections were washed three times (2 min each) with TBS and mounted with Prolong Gold antifade media formulated with DAPI (Thermo Fisher Scientific). The slides were protected from light and air-dried overnight at RT prior to imaging. Negative controls included omission of the primary antibody and incubation only with secondary antibody and SA-CY3. Images were captured on an Olympus IX81 inverted microscope using the 20× objective.

Detection of human IgG in mouse brain

Female mThy-1-α-syn mice (12 weeks old, 25–33 g) or male C57BL6/C3H mice (4 months old, 25–33 g) were intraperitoneally or intravenously administered either Grabody B-fused therapeutic antibodies or therapeutic antibodies alone. Approximately 4, 24, or 72 h after dosing, the animals were anesthetized with ketamine, perfused by PBS, and their brains extracted, drop-fixed in 4% paraformaldehyde overnight at 4°C, and placed in 30% sucrose overnight at 4°C. The brains were then sectioned at a thickness of 40 μm using a cryostat microtome, blocked in 5% BSA in 0.3% Triton X-100 (PBSX) for 1.5 h at RT, and stained with AlexaFluor488 goat-anti-human secondary antibodies (1:250, Jackson 109-545-003) and DAPI in 1% BSA in PBSX at room temperature for 2 h. Brain sections were washed in PBSX before mounting on slides and imaged using a laser scanning confocal microscope (LSM 800, Zeiss, Germany). The intracellular uptake of human IgG by cortical neurons was analyzed using Image J (version 1.50, NIH, USA).

Intravital imaging

For repetitive intravital imaging of brain tissues, a 3-mm-diameter cranial window was surgically implanted into an mThy-1-α-syn mouse as described previously (Holtmaat et al., 2009). To visualize whether the test antibodies cross the BBB, brain vessels were fluorescently labeled by intravenous injection of anti-CD31 Ab (clone 390; BioLegend, Cat#102402) conjugated with AlexaFlour555 (Thermo Fisher Scientific) 1 h before intravital brain imaging. The test antibodies were conjugated with Alexa Fluor 647 (Thermo Fisher Scientific), which were intravenously injected at 100 mg/kg via a tail vein catheter during the imaging. Using a commercial intravital confocal microscope (IVM-CM, IVIM Technology, South Korea), the distributions of the antibodies in the brain vasculature and parenchyma were repetitively visualized. Z-stack images were obtained at multiple spots and processed using two different types of area ratios.

IGF1R epitope mapping

IGF1R expression, mutant library, and cell-based screening

Recombinant human IGF1R fused with GFP at its N-terminus was cloned into a mammalian expression vector and transfected into OVCAR3 cells for protein expression. To screen the epitope(s) of IGF1R for anti-IGF1R antibody (clone #1564), a library was constructed of alanine mutation at an individual residue of the IGF1R ECD. Twenty-four hours post-transfection, the OVCAR3 cells expressing IGF1R were harvested and treated with the mutated anti-IGF1R antibodies. Cells were further stained using a DyLight650 anti-human secondary antibody, allowing for fluorescent detection of cells bound to the anti-IGF1R antibody by fluorescence-activated cell sorting (FACS). Resulting cells were split into two equal samples. The first sample was sorted for eGFP-positive cells, which included all cells expressing IGF1R. The second sample was sorted for cells exhibiting both the eGFP-positive and DyLight650-positive signals, which included all cells expressing IGF1R variants that bound to the mutated anti-IGF1R antibodies.

Next-generation sequencing

To identify IGF1R substitutions in each FACS-sorted cell pool, we conducted RNA sequencing in each cell population. For RNA sequencing, we first isolated mRNA from each cell population, converted the mRNA into cDNA by reverse transcription, and amplified the transfected IGF1R gene variants using primers against the N-terminal eGFP and 3′ end of IGF1R. Using IGF1R cDNA material, we built amplicons for regions with the alanine substitutions and deep-sequenced each amplicon using Illumina HiSeq technology. Deep sequencing data were processed to determine which IGF1R residues were critical for antibody binding through the effect of substituting each wild-type amino acid with alanine. For each sequencing amplicon, we first aligned raw Illumina sequencing data to the wild-type IGF1R sequence, followed by alanine mutation calling and variant counting. This provided us with the number of alanine counts at each mutation position for GFP + cells and GFP+/DyLight650 + cells. Alanine mutation counts were normalized to the wild-type sequencing count and then compared between GFP+ and GFP+/DyLight650 + cells. In the high signal-to-noise ratio screen, we managed to obtain binding data for ∼97% of all intended alanine substitutions. This is in contrast to the binding data for ∼75% of intended alanine substitutions in the first pass screen. We filtered the data for alanine substitutions that resulted in a significant change in the Log1 ratio between the GFP+/DyLight650+ and GFP+ only populations. As expected, alanine substitutions that are disruptive to anti-IGF1R antibody binding were enriched in the GFP+ populations compared to the GFP+/DyLight650 + populations.

Mass spectrometry and selected reaction monitoring (SRM)

Antibody levels in protein extracts from trans-well samples and serum, CSF, and brain samples were quantified using targeted, multiplexed mass spectrometry in selected reaction monitoring (SRM) mode as described previously (Farrington et al., 2014; Haqqani et al., 2008, 2013; Webster et al., 2016). Briefly, samples containing the antibodies were reduced, alkylated, and trypsin-digested using a previously described protocol. Peptide signatures for various antibody domains (hFc: TTPPVLDSDGSFFLYSK, ALPAPIEK, FNWYVDGVEVHNAK; Fab, GPSVFPLAPSSK, STSGGTAALGCLVK; anti-IGF1R, SGTASLAISGLR; anti-α-syn, ANDYT TEYSASVK) and endogenous marker (albumin: APQVSTPTLVEAAR) were identified, and an isotopically heavy version of the hFc peptide TTPPVLDSDGSFFLYSK (ILIS, +8 Da) was synthesized (New England Peptide LLC, Gardner, MA) as described previously (Haqqani et al., 2013). All signatures were validated in control matrix (serum, CSF, brain extracts) and antibody-spiked matrix to develop multiplexed SRM methods. For absolute quantification, calibration curves were created in antibody-spiked matrices (40–9600 nM plasma; 0–80 nM CSF; 0.3–45 nM). At least three quality control standards (low, mid, and high) were also prepared by independently spiking the antibodies in the appropriate matrices and run after every 5 to 10 samples. All samples were analyzed by nanoLC-SRM by injection onto a C18 PepMap^{TM} 100 trap (ThermoFisher, Waltham, MA) and subsequent nanoLC BEH130C18 column (Waters, Milford, MA) on a nanoAcquity UPLC (Waters) coupled with ESI-LTQ-XL-ETD or TSQ-Quantiva mass spectrometers (ThermoFisher). SRM methods were used with a combination of specific signatures to be monitored. Data were analyzed using Skyline software version 3.7 (https://skyline.ms) (MacLean et al., 2010). Albumin peptide was used to identify and exclude serum-contaminated CSF samples (albumin CSF/serum ratio >0.1%).

Immunostaining of human brains

Immunofluorescent staining of AD brains

Samples from the midfrontal cortex of three post-mortem AD patients (X5840, X5851, X58733) and three age-matched healthy controls (X5465F, X5510F, X6870F) were from the UCSD ADRC Brain Bank, embedded in paraffin, and sectioned at 7 μm. The sections

were stained with a mouse anti-IGF1R Ab (1:100 dilution; Santa Cruz, sc81167) and rabbit anti-CD31 Ab (1:200; Abcam, 28364). Goat anti-mouse IgG-Alexa568 (red) or anti-rabbit IgG-FITC (green) were used to visualize anti-IGF1R or anti-CD31. Images were captured under a 10× objective using a Leica SP8 confocal microscope, and 4–5 regions with a ROI of 720 × 720 μm^2 were randomly selected from each sample and the average immunofluorescence intensity measured using Image J.

Immunohistochemistry (IHC) and IF of normal brains

Paraffin-embedded blocks and snap frozen tissue blocks were obtained from the National Disease Research Interchange (NDRI) in the United States with acknowledgement of support from NIH grant U42OD11158.

Brain tissue sections were washed twice with PBS and blocked using 3% H_2O_2. Immunohistochemical detection was carried out using mouse anti-IGF1R Ab (1:100 dilution; Santa Cruz, sc81167) and the avidin-biotin complex (ABC) system (Vectastain ABC Elite Kit, Vector Laboratories, Burlingame, CA). Immunocomplexes were visualized with the 3,3′-diaminobenzidine (DAB) and obtained using an Olympus BX51 microscope mounted with a DP70 Olympus digital camera. Quantification was performed by ImageJ (version 1.50, NIH, USA).

For IF, the brain tissues were sectioned into 4-μm-thick slices, attached to a slide glass, deparaffinized with xylenes, and sequentially rehydrated with graded ethanol solution (100–70%). Antigen retrieval was performed by incubating sections in citrate-based antigen unmasking solution (pH 6.0) in a steam bath for 10 min. Endogenous peroxidase activity was quenched with 3% H_2O_2 containing 0.005% Triton-X-100 in PBS for 5 min. The sections were blocked with 2.5% normal serum in PBS, and then incubated with anti-IGF1Rα (Santa Cruz, sc-271606), anti-CD31 (Abcam, ab28364), and anti-NeuN (Abcam, ab177487) antibodies overnight at 4°C. After washing with PBS, the sections were incubated with anti-rabbit IgG Alexa Fluor 448 (Thermo Fisher Scientific, A21206) or anti-mouse IgG Alexa Fluor 564 (Thermo Fisher Scientific, A10036). The slides were cover-slipped using Vectashield mounting medium with DAPI and imaged using a Nikon A1 confocal laser microscope and NIS elements imaging software.

Western blot

MCF7 cells

MCF7 cells (0.4 × 10^6 cells) were seeded in growth medium on 6-well culture plates for 1 day. The cells were serum starved in DMEM/F-12 medium (Gibco) for 20 h. After serum starvation, the cells were co-stimulated with human IgG, M30103, B30104, or A12 (1–10 μM) and recombinant human IGF-1 (200 ng/mL, R&D systems, 291-G1) for 20 min. The cells were lysed in mammalian protein extraction reagent (M-PER; Fisher Scientific, 78501) with protease and phosphatase inhibitor cocktail (PIC; Pierce, 1861281). The cell lysates were separated on 4–12% Bis-Tris gels and transferred to PVDF membranes. Finally, the proteins were blotted with antibodies against phosphorylated-Akt (Cell Signaling, 9271S), total Akt (Cell Signaling, 9272S), phosphorylated-IGF1R (Cell Signaling, 3024S), total IGF1R (Cell Signaling, 3018S), and β-actin (Santa Cruz, Sc-47778).

Mouse tissues

Mice were sacrificed by ketamine overdoes and the brain and peripheral organs (pancreas, colon, liver, and heart) removed after transcardial perfusion with 20 mL of PBS. The tissues were immediately frozen by liquid nitrogen after removal and stored at −80°C until use. For capillary depletion of the brain, the right hemisphere was placed in ice cold PBS. The choroid plexuses were dissected and discarded. Brains were then homogenized in 3.5 mL HBSS containing protease and phosphatase inhibitors (Roche, 04693159001 and 04906837001) by 10 strokes with a Dounce homogenizer using only the smaller diameter pestle. The homogenate was centrifuged at 1,000 *g* for 10 min and the supernatant discarded. The pellet was resuspended in 2 mL of 17% dextran (MW 60,000; Sigma 31397), and then centrifuged at 4,122 *g* for 15 min. The resulting pellet contained the vasculature. The supernatant containing parenchymal cells and myelin was transferred to a new tube and diluted with HBSS, and then centrifuged at 4,122 *g* for 15 min; the supernatant was discarded, resulting in a pellet of the vascular-depleted parenchymal fraction. Both the vascular pellet and parenchymal pellet were resuspended in cold 1% NP40 in PBS containing protease and phosphatase inhibitors, vortexed for 20 s, and incubated at 4°C for 20 min. The samples were centrifuged at 12,700 *g* for 10 min and their total protein content measured using the BCA assay (Thermo, 23225).

The dissected peripheral tissues (liver, heart, pancreas, and colon) were weighed and extracted in RIPA buffer containing protease and phosphatase inhibitors (Roche). A total of 5 mL of buffer was used per gram of tissue. The samples were sonicated and cleared by centrifugation at 100,000 *g* for 30 min.

A total of 20 μg of sample per well was separated on SDS-polyacrylamide gels (4–20% gradient) and transferred to nitrocellulose membranes. The blots were blocked in 5% non-fat milk in TBS and probed against phosphorylated-Akt, total Akt, total IGF1R, and β-actin (identical to the ones used for Western blot of MCF7 cells). Protein bands were detected and quantified using the OdysseyClx infrared scanning system (Li Cor, Lincoln, Nebraska).

Post-mortem human brains

Human brains obtained from NDRI were prepared following a previous report, with some modifications (Moloney et al., 2010). The minced cortex was resuspended in 1 mL of hypotonic buffer (10 mM HEPES pH 7.5, 2 mM $MgCl_2$, 25 mM KCl, 0.5 mM EDTA, 0.5 mM EGTA, 1 mM DTT, 1 mM AEBSF, 5 μg/mL leupeptin and aprotinin, 1 mM Na_3VO_4, 5 mM NaF) and placed on ice for 30 min. The resuspended tissues were gently homogenized by 25 strokes in a Dounce homogenizer and the homogenates centrifuged twice at 750 *g* for 10 min. The first pellets were kept on ice for nuclei preparation. The supernatants were further centrifuged at 100,000 *g* for 1 h using a table-top ultracentrifuge (Beckman Coulter). The resulting second pellet and supernatant were designated the membrane and

cytosolic fractions. Membrane fractions were loaded and immune-blotted using the identical method for mouse tissues. The membrane was probed with anti-IGF1R antibody (Cell Signaling, 3018S) and anti-β-actin (Cell Signaling, 4970).

Treatment of PFF-injected mice

To assess the chronic efficacy of Grabody B and its effect on brain IGF1R levels, mice were treated with 15 mg/kg of hIgG or M30103 or an equal molar amount of B30104 (17.55 mg/kg) via weekly intraperitoneal injections from 7 days post-PFF injection (12 mice/treatment group, total 36 animals; total 24 injections). Six non-PFF-injected animals were treated with PBS and used as a negative control.

To measure brain and serum M30103 and B30104 levels by LC-SRM analysis and the potential effects on the brain and peripheral IGF1R signaling components using Western blot, 30 mg/kg of hIgG or M30103, or 35.1 mg/kg of B30104 was administered weekly (intraperitoneally) for 180 days from 90 days post-PFF injection (total 12 animals, n = 3/test article). Three non-PFF-injected animals were treated with PBS and included as negative controls.

IHC of PFF-injected mouse brains

Brain tissues (6 animals per group) were fixed with 4% paraformaldehyde for 24 h, and then moved into 30% sucrose for 3 days. The brain tissues were sliced into 40-μm-thick sections using a cryostat microtome (Leica, 2800N, Germany) following the free-floating method. The sections were immersed in storage solution (0.02 M phosphate buffer, sterile water, ethylene glycol, glycerin) and stored at −20°C until further use.

The brain tissue sections were washed twice with PBS, followed by blocking with 3% H_2O_2. Immunohistochemical detection was achieved using the ABC system (Vectastain ABC Elite Kit, Vector Laboratories, Burlingame, CA) with anti-pSer129-α-syn (S129; Abcam, ab51253) or anti-tyrosine hydroxylase (TH; Pel-Freez, 40101) antibody. The immunocomplexes were visualized with the DAB and images obtained using an Olympus BX51 microscope mounted with a DP70 Olympus digital camera. Quantification was performed using ImageJ.

For cell counts, four fields in each tissue and four tissues per specimen were measured and adjusted to the average per unit area of 1 mm^2. For the count of TH-positive neurons in the substantia nigra pars compacta (SNpc), the total number of cells was counted in five tissue slides including the SNpc per specimen (Tran et al., 2014).

Behavioral assessments

Behavioral tests were carried out 3 days after the 90 days or 180 days of antibody or vehicle injections to avoid stress. Mice were acclimatized to the testing environment 1 day before the actual experiment. All behavioral tests were performed by an investigator blinded to the treatment conditions.

Rotarod test

First, mice were trained on a rotating rod that accelerated from 4 rpm to 40 rpm over 5 min (MED-Associates Rotarod Apparatus). After two training sessions, a trial session followed once a day over 3 days. Latency to fall was recorded and averaged over three testing trials.

Wire hang test

Briefly, mice were placed on top of a stainless steel wire mesh (30 cm × 30 cm, 1 mm wire diameter, 1 cm hole) and then turned upside down to let them grip the wires. The wire mesh was stirred with a shaking apparatus to gradually increase the shaking frequency from 0 Hz to 100 Hz over 1 min. After one training session, two trial sessions followed in a day. Trials were stopped if mice remained on the wire mesh for more than 5 min. Latency to fall was recorded and averaged over two testing trials.

Ethical statement

All housing and experimental procedures involving the use of laboratory animals were approved by the Kyung Hee University Institutional Animal Care and Use Committee [KHUASP(GC)-19-090], the Institutional Animal Care and Use Committee of Kbio health, and the Institutional Animal Care and Use Committee of IVIM technology. Surgical and animal procedures were carried out by strictly following the NIH Guide for the Care and Use of Laboratory Animals.

QUANTIFICATION AND STATISTICAL ANALYSIS

Data are presented as mean ± standard error of the mean (SEM) or standard deviation (SD). Statistical analyses were performed and P-values calculated using Prism6 (GraphPad Software, La Jolla, CA). The following statistical methods were used: unpaired t-test for pairwise comparisons of different groups, paired t-test for different means from the same subjects, one-way ANOVA for comparisons between multiple groups, and two-way ANOVA for multiple comparisons. P-values < 0.05 were considered significant, and P-values < 0.01 were considered highly significant.

Cell Reports Methods, Volume *2*

Supplemental information

Grabody B, an IGF1 receptor-based shuttle, mediates efficient delivery of biologics across the blood-brain barrier

Jung-Won Shin, Sungwon An, Dongin Kim, Hyunjoo Kim, Jinhyung Ahn, Jaehyun Eom, Weon-Kyoo You, Hyesu Yun, Bora Lee, Byungje Sung, Jinwon Jung, Sehyun Kim, Yonggyu Son, Eunsil Sung, Hanbyul Lee, Suyeon Lee, Daehae Song, Youngdon Pak, Jagdeep K. Sandhu, Arsalan S. Haqqani, Danica B. Stanimirovic, Jiseon Yoo, Donghwan Kim, Sungho Maeng, Jeonghun Lee, and Sang Hoon Lee

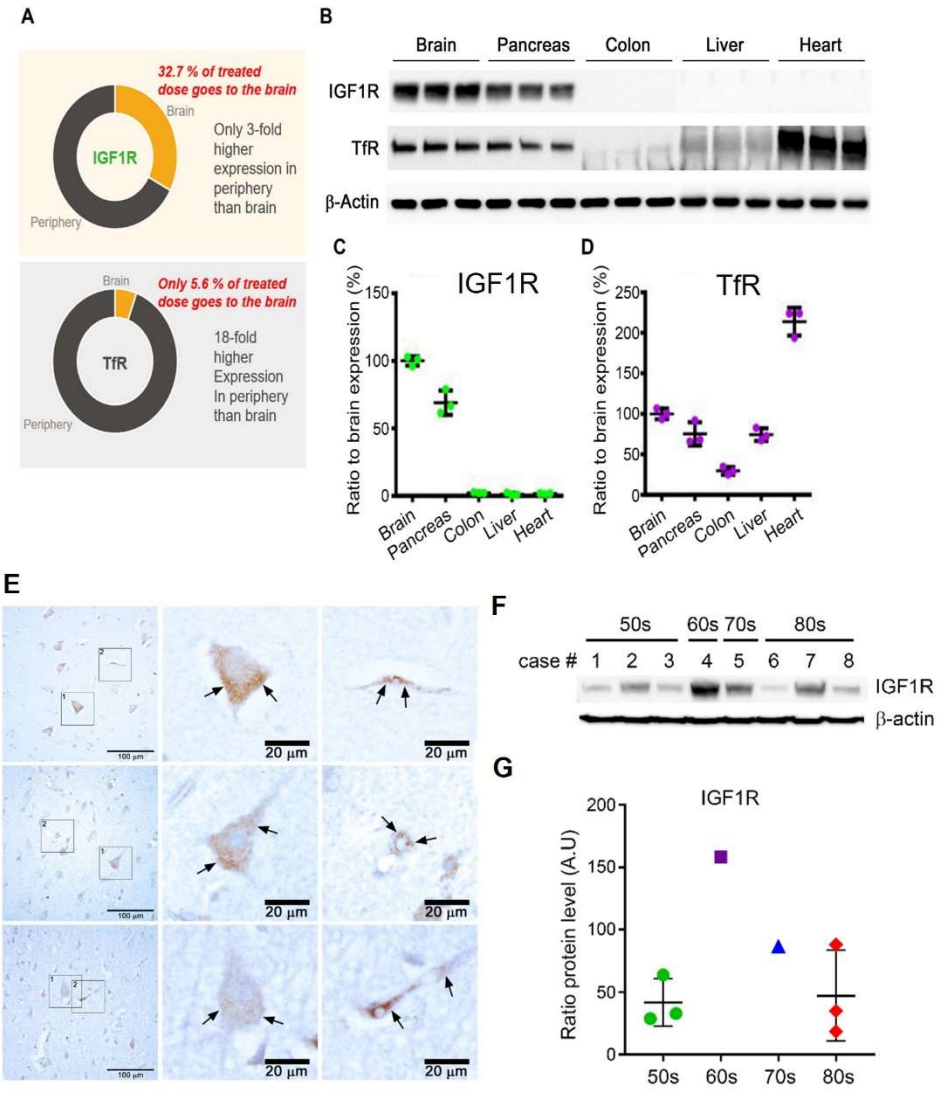

Figure S1. Brain IGF1R expression is higher than its peripheral expression, in contrast to the higher peripheral expression of TfR, Related to Figure 1.

(A) The absolute expression level of IGF1R and TfR in various tissues was obtained from a public database (https://pax-db.org) (Wang et al., 2012). PaxDB organized the expression level of targets as an absolute value called 'parts per million' in order to enable a direct comparison between targets. The expression levels in the brain, liver, lung, colon, esophagus, pancreas, and heart were summed together and compared to the target's expression in the brain (IGF1R_total: 9.02 ppm vs. IGF1R_brain: 2.22 ppm; TfR_total: 266.67 ppm vs. TfR_brain: 14 ppm). Due to high peripheral TfR expression, up to 18-fold more than its brain expression, a significant amount of therapeutic mAb fused with the anti-TfR shuttle may be systemically sunk. In contrast, brain IGF1R expression is approximately one-third the IGF1R expression in a system; thus, a bispecific antibody with a therapeutic mAb and anti-IGF1R shuttle may reach the CNS without losing too much in the periphery after intravenous dosing. (B) Immunoblot of lysates from five mouse organs (brain, pancreas, colon, liver, and heart) with either anti-IGF1R antibody or anti-TfR antibody. Notably, a minimal or absent IGF1R-positive band was observed in the colon, liver, and heart, whereas strong immunoreactivity to TfR was found in the three organs, especially the heart. (C, D)

Quantification of the band intensity in (B). An average intensity of three wells of brain samples was normalized to 100, and the relative band intensity of other organs was obtained. Data are presented as mean ± SEM. n = 3 mice. (E) Postmortem brains from three subjects (one in each row) showed clear IGF1R-immunoreactivity in brain cells (#1) and the brain microvessels (#2) (arrows). The middle and right columns are enlarged images of #1 and #2, respectively. Scale bar = 20 μm. (F) Western blot bands for IGF1R in postmortem brain tissues from different ages (50s: $n = 3$; 60s: $n = 1$; 70s: $n = 1$; 80s: $n = 3$; total $n = 8$). β-actin was used as a loading control. None of the 8 subjects had neurodegenerative diseases. Subject 4 (age: 60s) had a history of diabetes and related medication for years. (G) Quantification of the IGF1R bands after normalization to β-actin. The optical density of each band was averaged with the same group. Overall, three age groups showed similar IGF1R expression levels, implying that brain IGF1R levels are maintained (50s: green; 60s: purple; 70s: blue; 80s: red; One-way ANOVA, $p > 0.05$). Subject 4 was an outlier possibly because of the history of diabetes and medication, which could have increased the IGF1R expression. The line and whiskers indicate mean ± SD.

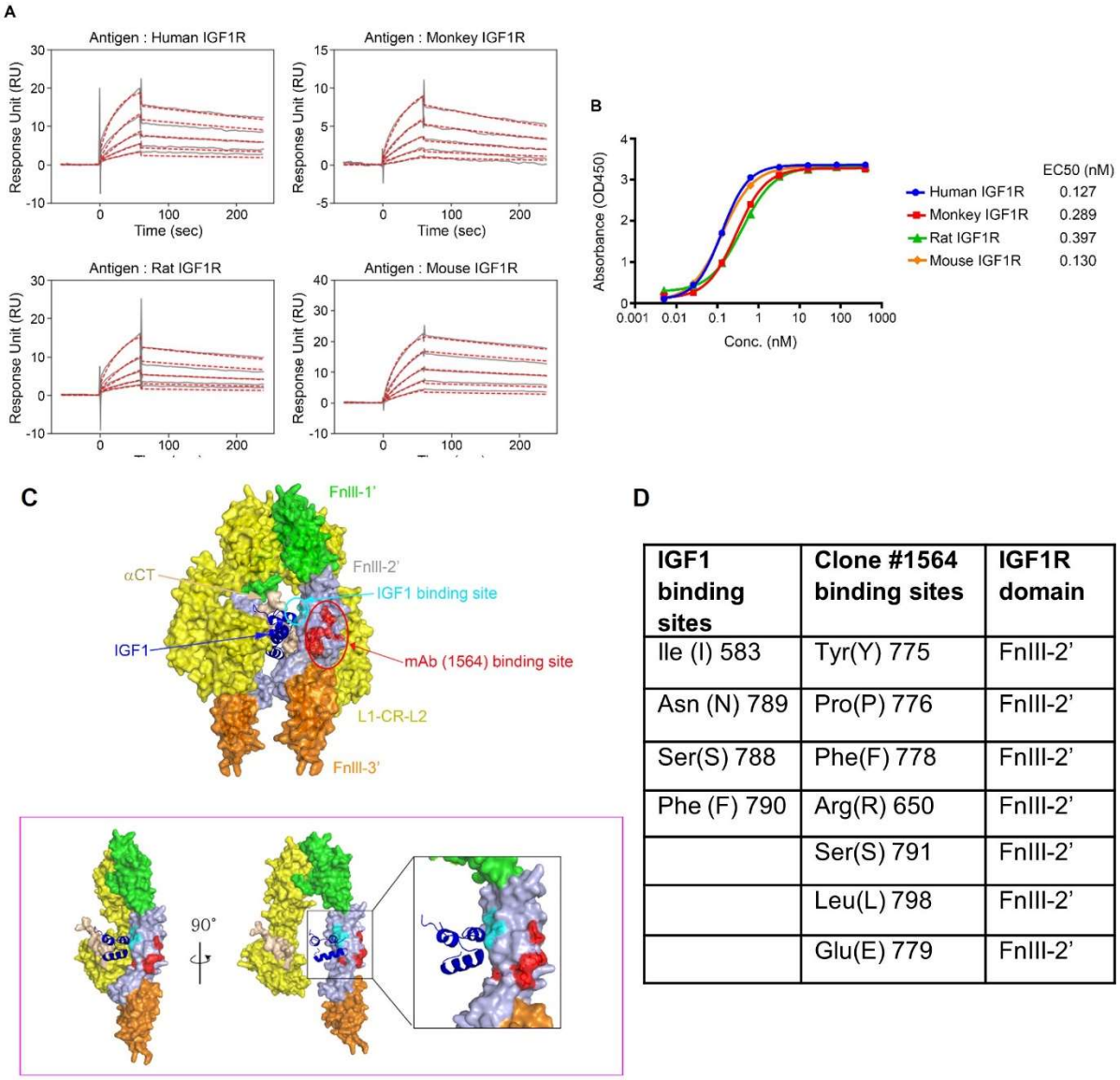

IGF1 binding sites	Clone #1564 binding sites	IGF1R domain
Ile (I) 583	Tyr(Y) 775	FnIII-2'
Asn (N) 789	Pro(P) 776	FnIII-2'
Ser(S) 788	Phe(F) 778	FnIII-2'
Phe (F) 790	Arg(R) 650	FnIII-2'
	Ser(S) 791	FnIII-2'
	Leu(L) 798	FnIII-2'
	Glu(E) 779	FnIII-2'

Figure S2. Grabody B is an IGF1R binder that has broad cross-reactivity to IGF1R across species, and its parental antibody (Clone #1564)'s IGF1R binding site indicates no interference with IGF1 binding site, Related to Figure 2.

(A) SPR sensorgram plot of B30104 (Grabody B-fused anti-α-Syn antibody) for the extracellular domain (ECD) of human, mouse, rat, and monkey IGF1R. Each panel shows an overlay plot of the measured response (grey color) with the global fit (red color). B30104 showed fairly similar binding kinetics to four different IGF1R proteins. (B) B30104 binding to the IGF1R ECD proteins from the four species in ELISA. B30104 showed similar binding profiles (EC50) between human (blue) and mouse (orange) IGF1R, and between monkey (red) and rat (green) IGF1R. (C) The structure of homo-dimeric IGF1Rs was obtained using PDB: 5U8Q (Xu et al., 2018) with each domain marked in different colors. The binding of IGF1 (dark blue) to its binding site on IGF1R (sky blue) is clearly visible. In contrast, the binding site of clone #1564 (red) is shown apart from the IGF1 binding site. Pink box: Monomeric IGF1R with the same color code. The enlarged image (inset) clearly describes the physical distance between the IGF1 binding site (sky blue) and the 1564 binding site (red), as it is consistent with the distance between the two binding sites (D).

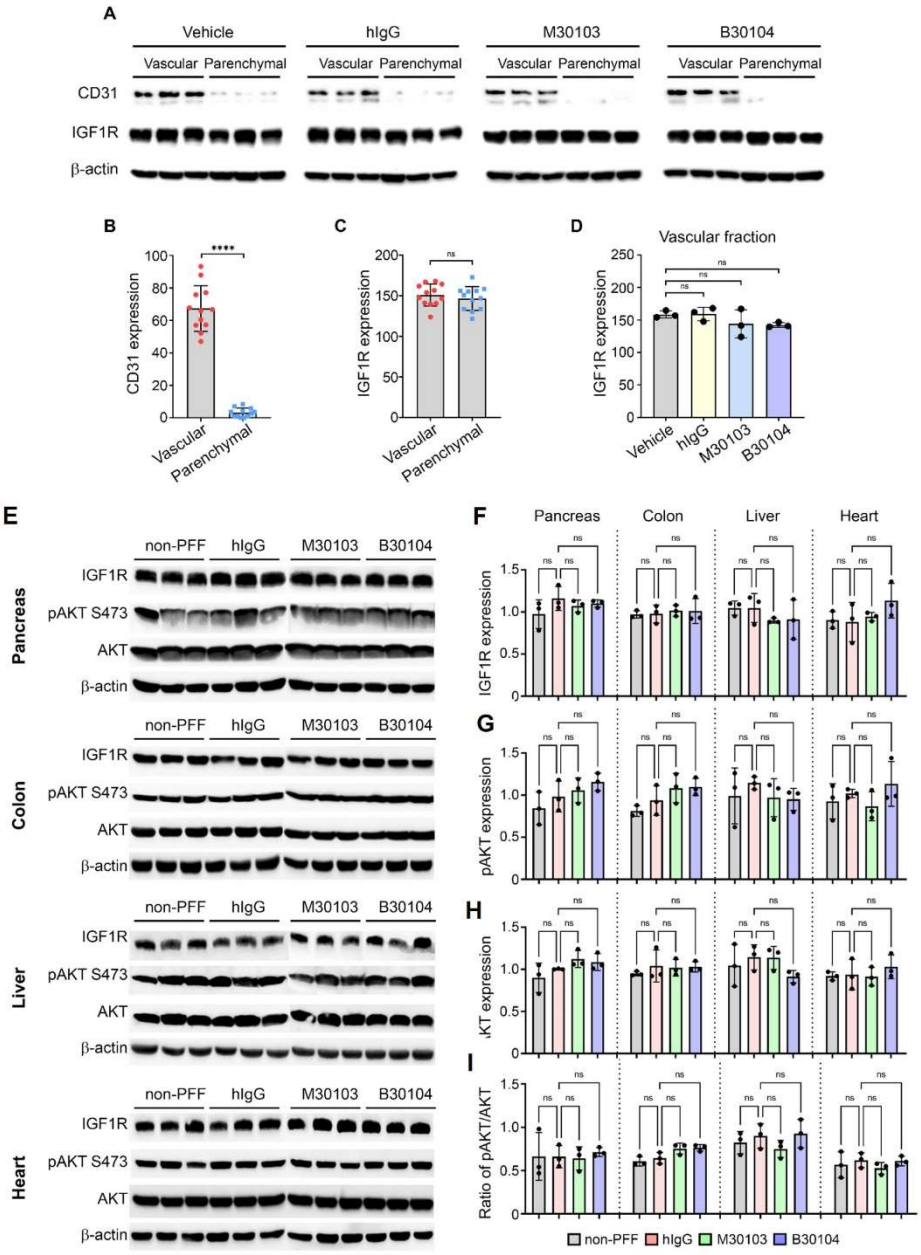

Figure S3. No significant changes in brain and peripheral IGF1R after repeated dosing with B30104, Related to Figure 2.

(A) Immunoblot bands for mouse brain vascular or parenchymal fractions treated with 30 mg/kg hIgG or M30103 or 35.1 mg/kg B30104 for 3 months. The IGF1R and CD31 levels in each fraction are shown as an immunoblot. β-actin was used as a loading control. (B) Quantification of the band intensity for CD31in all treated animals in (A). Note the lack of a band for CD31 in parenchymal fractions. (C) Quantification of the band intensity for brain IGF1R in all treated animals and (D) in individual treatment groups. Note the similar vascular IGF1R level between groups. Data are presented as mean ± SEM. B,C: paired t-test; D: ordinary one-way ANOVA, **** $p < 0.0001$, ns = not significant. (E) Immunoblot bands for total IGF1R, pAKT, and AKT in the pancreas, colon, liver, and heart of mice treated with weekly intraperitoneal doses of 30 mg/kg hIgG or M30103 or 35.1 mg/kg B30104 for 3 months. The mice, except the non-PFF control group, were injected in the striatum with PFF 3 months prior to the antibody dosing. (F-H) Quantification of the band intensity in (E). Data are presented as mean ± SD; n = 3 per treatment. ns = not significant; ordinary one-way ANOVA. (I) Ratio of the pAKT- and AKT-immunoreactive band intensity. Data are presented as mean ± SD; n = 3 per treatment. ns = not significant, ordinary one-way ANOVA.

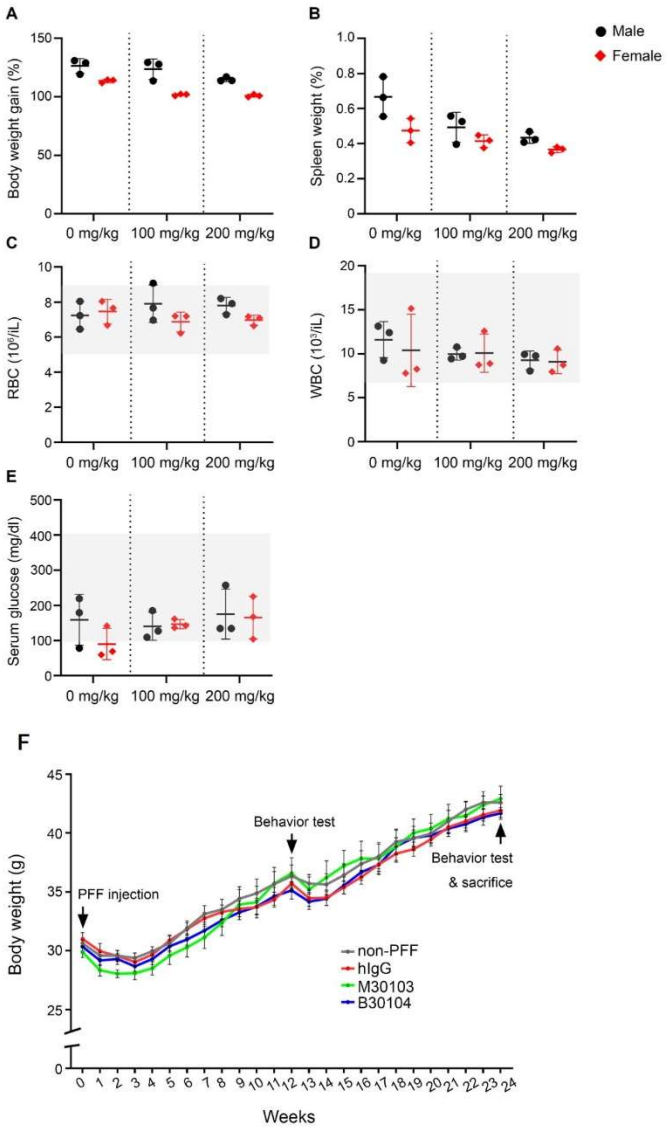

Figure S4. B30104 induces no drug-related adverse events in rats and PFF-injected mice with repeated dosing, Related to Figure 2.

Six SD rats (3 males, black circles; and 3 females, red diamonds) received vehicle or 100 mg/kg or 200 mg/kg of B30104 weekly for 2 weeks. The body weight (A), spleen weight (B), red blood cells (C), white blood cells (D), and serum glucose levels (E) of the two groups treated with B30104 were comparable to the vehicle group (0 mg/kg). Data are presented as mean ± SD; n = 6. (F) The weight of the PFF-injected mice in Figure 7-9 was monitored during 24 weeks with weekly intraperitoneal administration of 15 mg/kg hIgG or M30103 or 17.55 mg/kg B30104. The four groups, including the non-PFF control, had overall similar weight over the 24 weeks. Data are presented as mean ± SEM; n = 12 per treatment. ns = not significant; ordinary one-way ANOVA.

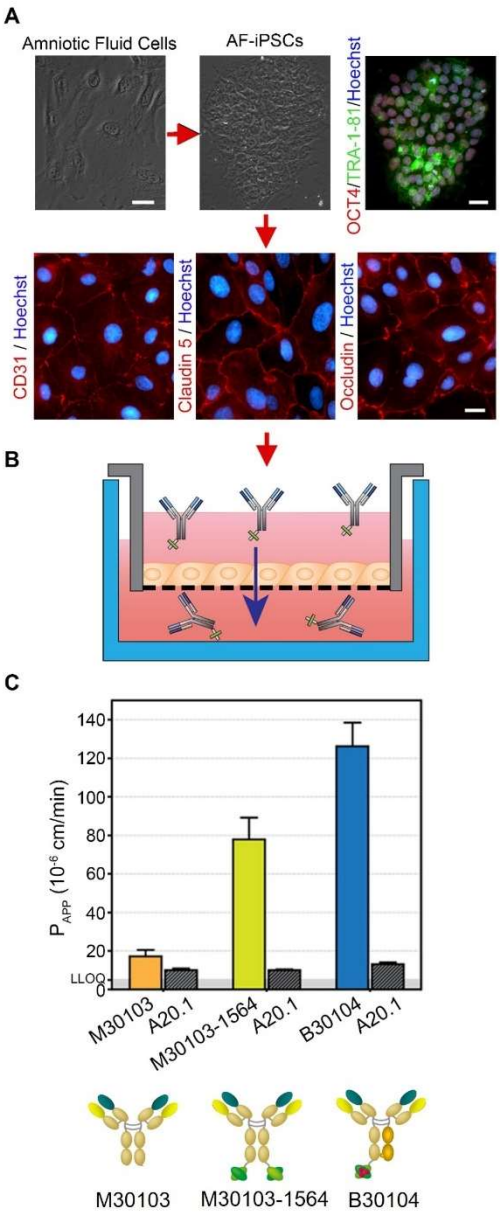

Figure S5. Grabody B mediates efficient transcytosis in a trans-well system, Related to Figure 3.
(A) Schematic of the induced brain endothelial cells (iBECs) differentiated from human amniotic fluid-derived induced pluripotent stem cells (AF-iPSCs). Scale bar = 20 μm. (B) Illustration of the trans-well assay using the AF-iPSCs. (C) Apparent permeability coefficient (Papp) of three antibodies (M30103, yellow; M30103-1564 bivalent, green; and B30104, blue) in the iBEC in vitro BBB model. Single-domain antibody A20.1 (hashed bars, negative control) against a non-mammalian target was used to confirm the trans-well's selective permeability. Data are presented as mean ± SD for at least three independent trans-well inserts.

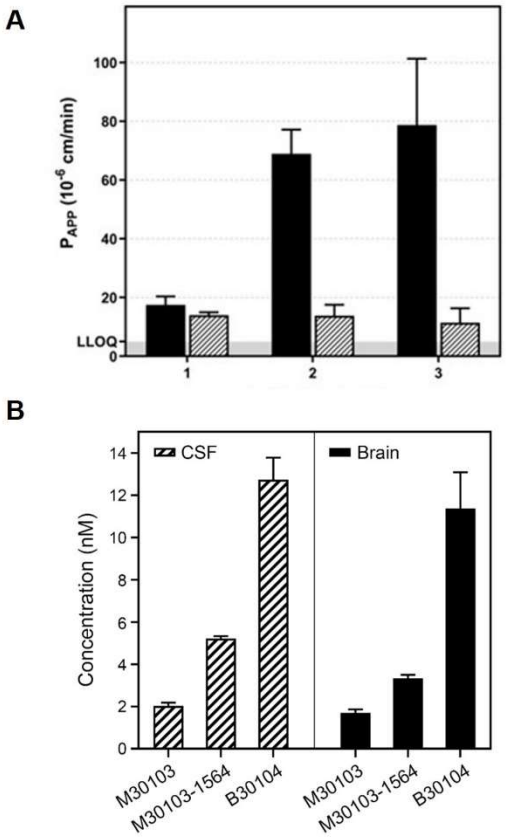

C

Parameters	Units	M30103	B30104
Serum AUC_{0-T}	hr*nmol/ml	301.8	306.6
CSF AUC_{0-T}	hr*nmol/ml	0.159	0.918
Brain AUC_{0-T}	hr*nmol/ml	0.134	1.116
CSF AUC_{0-T}/Serum AUC_{0-T}	%	0.053	0.299
Brain AUC_{0-T}/Serum AUC_{0-T}	%	0.044	0.364

Figure S6. *In vitro* and *in vivo* assessment of BBB penetration by Grabody B using SV-ARBECs and rats, Related to Figure 3 and 4.

(A) Apparent permeability coefficient (Papp) of three antibodies in the rat SV-ARBEC *in vitro* BBB model. The antibodies (filled bars) refer to M30103 (#1), M30103-1564 bivalent (#2), and B30104 (#3). Single-domain antibody A20.1 (hashed bars) was used in each trans-well insert as an 'in-experiment' control for endothelial monolayer permeability. Data are presented as mean ± SD of at least three independent trans-well inserts. (B) CSF and brain hIgG levels measured by LC-SRM 24 hours after a single intravenous dose of 30 mg/kg M30103 or the molar equivalent dose of M30103-1564 bivalent, B30104 to rats. Data are presented as mean ± SD; n = 3 rats per treatment. (C) Rat PK profile of M30103 and B30104 shown in Figure 4.

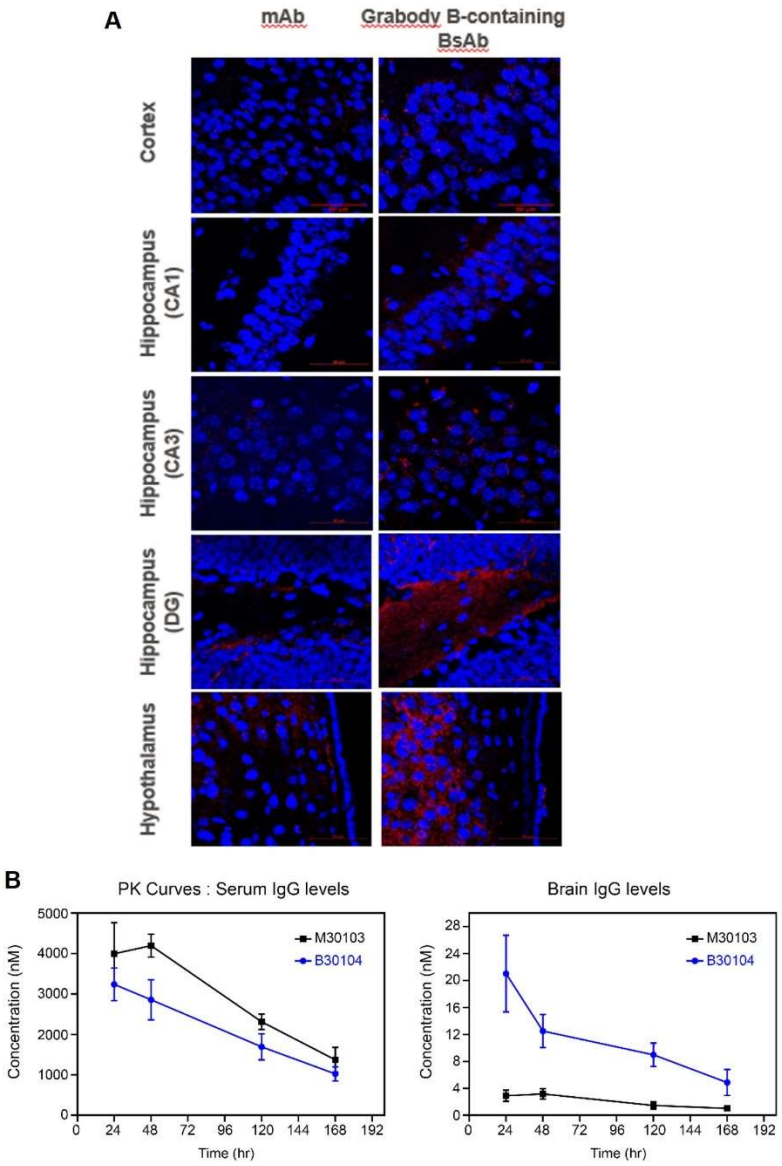

Figure S7. Increased brain level of Grabody B-fused antibody compared to monoclonal antibody in mice, Related to Figure 4-7.

(A) Immunostaining of mouse brain sections after a single intravenous injection of monoclonal antibody targeting BACE1 at 50 mg/kg or the same molar concentration of Grabody B-containing anti-BACE1 bispecific antibody. Note the higher intensity signal of Grabody B-fused anti-BACE1 antibody from 72 hours post-injection compared to anti-BACE1 antibody in four different brain areas. (B) Serum and brain levels of M30103 and B30104 in PFF-injected mice. M30103 at a dose of 30 mg/kg or the molar equivalent of B30104 was administered intraperitoneally to the PFF-injected mice weekly for 3 months. The dosing was initiated 3 months after PFF injection. Serum and brains were collected from mice at four different time points (24, 48, 120, and 168 hours) after the last dosing, and their hIgG level was analyzed using LC-SRM. B30104 was present at comparable or slightly lower levels in serum than M30103. In the brain, the B30104 level was significantly higher at all four time points than the M30103 level, suggesting that the better efficacy of B30104's could potentially be driven by the elevated brain exposure to B30104 (Time points: $p = 0.0079$; M30103 vs. B30104: $p < 0.0001$; Two-way ANOVA). Data are presented as mean ± SD.